

# 1 Cloud top pressure retrieval with DSCOVER-EPIC oxygen A and B bands observation

2 Bangsheng Yin<sup>1</sup>, Qilong Min<sup>1,\*</sup>, Emily Morgan<sup>1</sup>, Yuekui Yang<sup>2</sup>, Alexander Marshak<sup>2</sup>, and  
3 Anthony B. Davis<sup>3</sup>

4  
5 <sup>1</sup>Atmospheric Sciences Research Center, University at Albany, Albany, NY, USA

6 <sup>2</sup>NASA Goddard Space Flight Center, Climate and Radiation Laboratory, Greenbelt, MD,  
7 USA

8 <sup>3</sup>Jet Propulsion Laboratory, California Institute of Technology, Pasadena, CA, USA

9  
10  
11 \* Corresponding author, qmin@albany.edu

## 12 13 Abstract

14 An analytic transfer inverse model for Earth Polychromatic Imaging Camera (EPIC)  
15 observation ~~was~~is proposed to retrieve the cloud top pressure (CTP) with considering in-cloud  
16 photon penetration. In this model, an analytic equation was developed to represent the reflection  
17 at top of atmosphere (TOA) from above cloud, in-cloud, and below-cloud. The coefficients of  
18 this analytic equation can be derived from a series of EPIC simulations under different  
19 atmospheric conditions using a non-linear regression algorithm. With estimated cloud pressure  
20 thickness, the CTP can be retrieved from EPIC observation data by solving the analytic equation.  
21 To simulate the EPIC measurements, a program package using the double-*k* approach was  
22 developed. Compared to line-by-line calculation, which this approach can calculate high-  
23 accuracy results with a one-hundred-fold computation time reduction. During the retrieval  
24 processes, two kinds of retrieval results, i.e., baseline CTP and retrieved CTP, are provided. The  
25 baseline CTP is derived without considering in-cloud photon penetration, and the retrieved CTP  
26 is derived by solving the analytic equation, taking into consideration the in-cloud and below-  
27 cloud interactions. The retrieved CTP for the oxygen A and B bands are smaller than their  
28 related baseline CTP. At the same time, both baseline CTP and retrieved CTP at the oxygen B-  
29 band are ~~obviously~~ larger than those at the oxygen A-band. Compared to the difference of  
30 baseline CTP between the B-band and A-band, the difference of retrieved CTP between these  
31 two bands is generally reduced. Out of around 10000 cases, in retrieved CTP between A- and B-  
32 bands we found an average bias of 93 mb with standard deviation of 81 mb. The cloud layer top  
33 pressure from Cloud-Aerosol Lidar and Infrared Pathfinder Satellite Observations measurements  
34 is used to do validation. Under single-layer cloud situations, the retrieved CTPs for the oxygen  
35 A-band agree well with the CTPs from CALIPSO, which mean difference is within 5 mb in the  
36 case study. Under multiple-layer cloud situations, the CTPs derived from EPIC measurements  
37 may be larger than the CTPs of high level thin-clouds due to the effect of photon penetration.

## 39 1. Introduction

40 The Deep-Space Climate Observatory (DSCOVR) satellite is an observation platform  
41 orbiting within the first Sun-Earth Lagrange point (L1), 1.5 million km from the Earth, carrying a  
42 suite of instruments oriented both Earthward and sunward. One of the Earthward instruments is  
43 the Earth Polychromatic Imaging Camera (EPIC) sensor, which can take images of the Earth  
44 with spatial resolution of 10 km at nadir. The EPIC continuously monitors the entire sunlit Earth  
45 for backscatter, with a nearly constant scattering angle between 168.5° and 175.5°, from sunrise  
46 to sunset with 10 narrowband filters: 317, 325, 340, 388, 443, 552, 680, 688, 764 and 779 nm  
47 (Marshak et al., 2018). Of the 10 narrow-band channels, there are two oxygen absorption and  
48 reference pairs, 764nm versus 779.5nm and 680nm versus 687.75nm, for oxygen A and B bands.  
49 The cloud top pressure (CTP) or cloud top height (CTH) is an important cloud property for  
50 climate and weather studies. Based on differential oxygen absorption, both EPIC oxygen A-band  
51 and B-band pairs can be used to retrieve CTP. It is worth noting that although CTP and CTH  
52 reference the same characteristic of clouds, the conversion between the two depends on their  
53 related atmospheric profiles.

54 Although the theory of using oxygen absorption bands to retrieve CTP was proposed  
55 decades ago (Yamamoto and Wark, 1961), it is still very challenging to do the retrieval  
56 accurately due to the complicated in-cloud penetration effect (Yang et al., 2019, 2013; Davis et  
57 al., 2018a, 2018b; Richardson and Stephens, 2018; Loyola et al., 2018; Lelli et al., 2014, 2012;  
58 Schuessler et al., 2013; Rozanov and Kokhanovsky, 2004; Kokhanovsky and Rozanov, 2004;  
59 Kuze and Chance, 1994; O'brien and Mitchell, 1992; Fischer and Grassl, 1991; and etc.). To  
60 estimate the CTP from satellite measurements, ~~Many-many~~ approaches ~~are~~ ~~have been~~ designed  
61 to retrieve clouds' effective top pressures without considering ~~their~~ in-cloud photon penetration.  
62 These approaches did not consider light penetrating cloud, and therefore the derived CTH is  
63 lower than the cloud top, ~~derive and the~~ effective top pressures ~~is~~ higher than CTP. In the  
64 meantime, to improve the retrieval accuracy of CTP, various techniques have been applied to the  
65 retrieval methods with in-cloud photon penetration. For example, Kokhanovsky and Rozanov  
66 (2004) proposed a simple semi-analytical model for calculation of the top-of-atmosphere (TOA)  
67 reflectance of an underlying surface-atmosphere system, accounting both for aerosol and cloud  
68 scattering. Based on the work of Kokhanovsky and Rozanov (2004), Rozanov and Kokhanovsky  
69 (2004) developed an asymptotic algorithm for the CTH and the geometrical thickness  
70 determination using measurements of the cloud reflection function. This retrieval method was  
71 applied by Lelli et al. (2012, 2014) to derive CTH using measurements from GOME instrument  
72 on board the ESA ERS-2 space platform.

73 Currently, based on the measurements of DSCOVR EPIC sensor, the Atmospheric Science  
74 Data Center (ASDC) at National Aeronautics and Space Administration (NASA) Langley  
75 Research Center archives both calibrated EPIC reflectance ratio data and processed Level 2  
76 cloud retrieval products, including cloud cover, cloud optical depth (COD), cloud effective top  
77 pressure at oxygen A and B bands (Yang et al., 2019). By using EPIC reflectance ratio data at  
78 oxygen A-band and B-band absorption to reference channels, Yang et al (2013) developed a  
79 method to retrieve CTH and cloud geometrical thickness simultaneously for fully cloudy scene  
80 over ocean surface. First their method calculates cloud centroid heights for both A- and B-band  
81 channels using the ratios between the reflectance of the absorption and reference channels, then  
82 derives the CTH and the cloud geometrical thickness from the two dimensional look up tables  
83 that relate the sum and the difference between the retrieved centroid heights for A- and B-bands

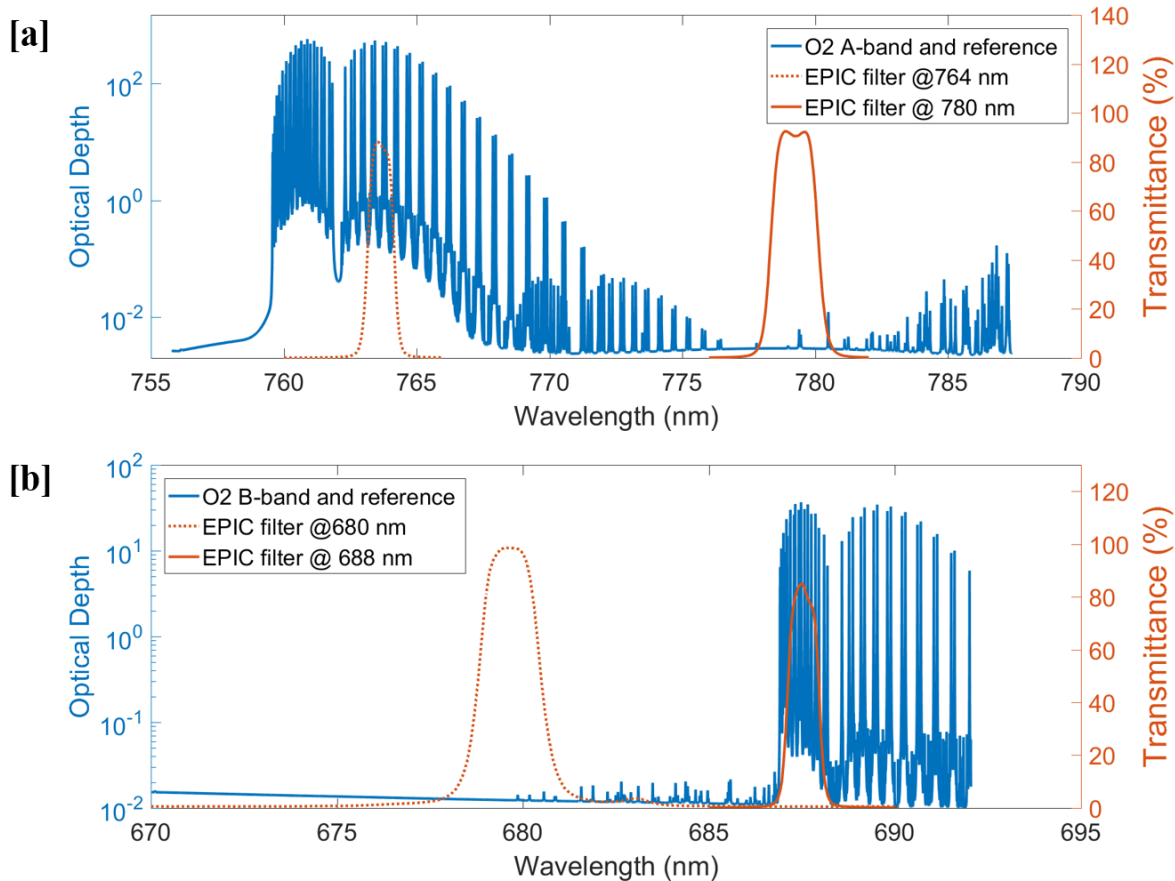
84 to the CTH and the cloud geometrical thickness. The difference in the O<sub>2</sub> A- and B-band cloud  
85 centroid heights is resulted from the different penetration depths of the two bands. Compared to  
86 the cloud height variability, the penetration depth differences are much smaller and the retrieval  
87 accuracy from this method can be affected by the instrument noise (Davis et al. 2018a, b).

88 In this paper, to address the issue of in-cloud penetration, we proposed an analytic method  
89 to retrieve the CTP by using DSCOVER EPIC oxygen A- and B-band observation. This analytical  
90 method adopted ideas of the semi-analytical model (Kokhanovsky and Rozanov, 2004; Rozanov  
91 and Kokhanovsky, 2004), and developed a quadratic EPIC analytic radiative transfer equation to  
92 analyze the radiative transfer in oxygen A- and B-band channels. The structure of this paper is as  
93 follows: section 2 describes the theory and methods, which includes several subsections, i.e., the  
94 introduction of absorption optical depth spectrum at oxygen A and B bands with their related  
95 DSCOVER EPIC oxygen A and B bands filters, the theory of CTP retrieval based on EPIC  
96 oxygen A- and B- band observation, and the detailed retrieval algorithm; section 3 describes the  
97 application and validation of the CTP retrieval method, which also includes several subsections,  
98 i.e., case studies of CTP retrieval, validation of the retrieval method, and retrieval of global  
99 observation;~~states the theory of CTP retrieval based on EPIC oxygen A-band and B-band~~  
100 ~~observation, section 4 describes the retrieval algorithms in detail with case studies and examples~~  
101 ~~of global observation data retrieval,~~ and section ~~5-4~~ states the conclusions of this study.

## 103 2. Theory and methods

### 104 2.1 DSCOVER EPIC oxygen A and B bands filters

105 EPIC filters at 764 nm and 779 nm cover the oxygen A-band absorption and reference  
106 bands, respectively (Figure 1a). The high resolution absorption optical depth spectrum at oxygen  
107 A-band and B-band is calculated by Line-By-Line Radiative Transfer Model (LBLRTM, Clough  
108 et al., 2005) with HITRAN 2016 database (Gordon et al., 2017) for the U.S. standard  
109 atmosphere. In this wavelength range, the O<sub>3</sub> absorption is very weak (O<sub>3</sub> optical depth < 0.003)  
110 and there are no other gas absorptions. The background aerosol and Rayleigh scattering optical  
111 depth vary smoothly within the A-band range; the differences between in-band and reference  
112 band are negligible at nominal EPIC response functions. EPIC filters at 688 nm and 680 nm  
113 cover the oxygen B-band absorption and reference band, respectively (Figure 1b). Compared to  
114 the oxygen A-band, O<sub>3</sub> absorption is slightly stronger in the oxygen B-band range, with an O<sub>3</sub>  
115 optical depth around 0.01. Any water vapor absorption in the B-band range is negligible. In the  
116 standard atmospheric model, from the oxygen B-band reference band to the absorption band, the  
117 O<sub>3</sub> absorption and Rayleigh scattering optical depth decreased by approximately 0.002 and  
118 0.002, respectively. This may have some impacts on the CTP retrieval from the oxygen B-band  
119 (more discussion in the later sections). It is worth noting that for EPIC measurements at both  
120 oxygen A- and B-bands, the surface influence cannot be ignoredis non-ignorable. For examples,  
121 in the snow or ice covered area the surface albedo is high; in the plants covered area, the surface  
122 albedo changes substantially between oxygen A-band and B-band due to the impact of spectral  
123 red-edge (Seager et al., 2005).



124  
125

126 **Figure 1:** High resolution calculated absorption optical depth spectrum at oxygen A-band (a)  
127 and B-band (b) with DSCOVr EPIC oxygen A and B bands in-band and reference filters. [Here](#)  
128 [the absorption optical depth spectrum is calculated by LBLRTM model with HITRAN 2016](#)  
129 [database for the U.S. standard atmosphere.](#)

130 In general, if we use the pair of oxygen A and B absorption and reference bands together,  
131 the impact of other absorption lines, background Rayleigh scattering, and aerosol optical depth  
132 are very limited. At the same time, as a well-mixed major atmospheric component, the vertical  
133 distribution of oxygen in the atmosphere is very stable under varying atmospheric conditions.  
134 Thus, we can use the ratio of reflected radiance (or reflectance) at the top of atmosphere (TOA)  
135 of oxygen absorption and reference bands (*i.e.*,  $R_{764}$  and  $R_{779}$ ,  $R_{688}$  and  $R_{680}$ ) to study the  
136 photon path length distribution and derive the cloud information. Also, [compared to any specific](#)  
137 [EPIC oxygen absorption bands \(\*i.e.\*,  \$R\_{764}\$  and  \$R\_{688}\$ \)](#), the ratios of absorption to reference  
138 [channels \(\*i.e.\*,  \$R\_{764}/R\_{779}\$  and  \$R\_{688}/R\_{680}\$ \)](#) are less impacted by the instrument calibration and  
139 other measurement error. [This can be explained by the following reasons: First](#), [the EPIC](#)  
140 [measurements at oxygen A and B absorption and reference bands share same sensor and optical](#)  
141 [system, when calculating the ratios of them, some preprocessing calibration errors can be](#)  
142 [reduced. Second](#), [to calculate  \$R\_{764}\$  and  \$R\_{688}\$ , the ratio of lunar reflectance at neighboring](#)  
143 [channels \(\*i.e.\*,  \$F\(764,779\)\$  and  \$F\(688,680\)\$ \) and the calibration factors of oxygen A and B](#)  
144 [reference bands \(\*i.e.\*,  \$K\_{779}\$  and  \$K\_{680}\$ \) are used \(\[Geogdzhayev and Marshak, 2018; Marshak et al.,\]\(#\)](#)  
145 [2018\).](#) Therefore, the accuracy of  $R_{764}$  and  $R_{688}$  is determined by the stability of  $F(764,779)$

146 [and  \$F\(688,680\)\$  and the accuracy of  \$K\_{779}\$  and  \$K\_{680}\$  together. But the accuracy of \[ratios of\]\(#\)  
147 \[absorption/ to reference ratios\]\(#\) is only determined by the stability of  \$F\(764,779\)\$   
148 \[and  \\$F\\(688,680\\)\\$ .\]\(#\)](#)

## 150 **2.2 Theory of CTP retrieval based on EPIC oxygen A- and B- band observation**

151 In our study, we tried two methods to retrieve the CTP based on EPIC oxygen A-band and  
152 B-band measurements: (1) Build a lookup table (LUT) for various atmospheric conditions and do  
153 the retrieval by searching the LUT; (2) Develop an analytic transfer [inverse](#) model for EPIC  
154 observations and calculate the related coefficients based on a series of simulated values, then use  
155 this analytic transfer [inverse](#) model to retrieve the CTP. In this paper, we mainly focus on the  
156 second method.

### 157 **3.2.1 Method 1: LUT based approach**

158 One commonly used method of retrieval for satellite observation is through the building  
159 and usage of LUTs ([Loyola et al., 2018](#), [Gastellu-Etchegorry and Esteve, 2003](#)). [LUT based](#)  
160 [approach can be fast because the most computationally expensive part of the inversion procedure](#)  
161 [is completed before the retrieval itself.](#) For DSCOVER EPIC observations, we can build ~~a~~-LUTs  
162 by simulating ~~the~~ EPIC measurements under various atmospheric conditions, such as different  
163 surface albedo, solar zenith and viewing angles, ~~cloud optical depth~~COD, CTP, and cloud  
164 pressure thickness. [Comparing the related simulated reflectance at the oxygen absorption and](#)  
165 [reference bands, we can obtain two LUTs for reflectance ratios of absorption/reference at EPIC](#)  
166 [oxygen A-band and B-band respectively, which can be used for the CTP retrieval. The detailed](#)  
167 [information of simulated reflectance ratio of absorption/reference is stated in Section 2.3.3.](#)

168 During the retrieval process, the EPIC measurements (e.g., reflectance at oxygen A and B  
169 bands) with related solar zenith and viewing angles can be obtained from the EPIC level 1B data;  
170 ~~cloud optical depth~~COD information (retrieved from other EPIC channels) can be obtained from  
171 EPIC level 2 data. At the same time, we can get surface albedo from Global Ozone Monitoring  
172 Experiment 2 (GOME-2) Surface Lambertian-equivalent reflectivity (LER) data (Tilstra et al.,  
173 2017). At this point the CTP and cloud pressure thickness are the only unknown variables. [The](#)  
174 [cloud pressure thickness or the cloud vertical distribution has substantial impact on the accuracy](#)  
175 [of the CTP retrievals \(Carbajal Henken et al., 2015; Fischer and Grassl, 1991; Rozanov and](#)  
176 [Kokhanovsky, 2004; Preusker and Lindstrot, 2009\).](#) In this study, the cloud pressure thickness is  
177 used as an input parameter to retrieve the CTP. However, no [related](#) accurate cloud pressure  
178 [thickness is provided by other satellite sensors now. To constrain the error ~~off~~from the estimation](#)  
179 [of cloud pressure thickness, we related it to the cloud optical thickness. It is reasonable because](#)  
180 [clouds with higher optical thickness normally have higher values of pressure thickness. To](#)  
181 [explore the correlation between cloud pressure thickness and cloud optical thickness, we use the](#)  
182 [related cloud data from Modern-Era Retrospective analysis for Research and Applications](#)  
183 [Version 2 \(MERRA-2, \[Gelaro et al., 2017\]\(#\)\), which is a NASA atmospheric reanalysis for the](#)  
184 [satellite era using the Goddard Earth Observing System Model Version 5 \(GEOS-5\) with](#)  
185 [Atmospheric Data Assimilation System \(ADAS\). Based on statistical analysis of one year's](#)  
186 [single-layer liquid water clouds over an oceanic region \(S23.20, W170.86, S2.11, W144.14\) in](#)

187 2017, we can get an equation for cloud pressure thickness approximation, i.e., cloud pressure  
188 thickness (mb) = 2.5\* COD + 23. The derived correlation coefficients ~~is~~ are dependent on the  
189 case region and time selections. ~~In the meantime, d~~Due to the complexity of cloud vertical  
190 distribution ~~in the atmosphere~~, whatever the accuracy of the correlation coefficients is, the  
191 estimation will certainly bring in error. ~~Cloud pressure thickness can be estimated with cloud~~  
192 optical thickness using statistical rules.

193 With an estimated cloud pressure thickness, ~~A~~ a multi-variable LUT searching method  
194 can then be used to interpolate and obtain the CTP. It is worth noting that the reflectance ratio of  
195 absorption/reference can be seen as a function of surface albedo, solar zenith and viewing angles,  
196 COD, CTP, and cloud pressure thickness. ~~certain~~ Some atmospheric variables will have a non-  
197 linear effect on the reflectance ratio. For example, the reflectance ratio is more sensitive to the  
198 variation of COD when COD is small. Overall, the reflectance ratio ~~varies~~ varies monotonically and  
199 smoothly with these variables (shown in Figure 3). ~~EPIC observations, however, these variations~~  
200 ~~occur smoothly~~. With a relatively high-resolution simulated table, we can use a localized linear  
201 interpolation method to estimate the proper values. Multiple interpolations are needed for this  
202 method to decrease the number of LUT dimensions, which will cost more time than the analytic  
203 transfer ~~inverse~~ model method. The retrieval error of this method is determined by the resolution  
204 of the LUT, i.e., the higher the resolution, the higher retrieval accuracy. However, for multiple  
205 dimensional LUTs, the increase of resolution will increase the table size exponentially, which  
206 will increase computational cost substantially for the table building and inverse searching.  
207 Another possible method to increase the retrieval accuracy is using different interpolation  
208 methods. For example, if the value of LUT varies non-linearly with a variable, using high order  
209 interpolation method maybe better than using linear interpolation method (Dannenberg, 1998). ~~In~~  
210 physics, the retrieval accuracy is impacted by two main uncertainty sources: (1) the limited  
211 ability of EPIC in identifying cloud thermodynamic phase, which will affect the accuracy of  
212 cloud optical thickness retrieval, and 2) the uncertainty in estimating Cloud pressure.

### 213 **2.23.2 Method 2: Analytic transfer inverse model**

214 For a long time, various efforts have been devoted to the study of radiative transfer in the  
215 atmosphere, including scattering, absorption, emission, and etc. (Chandrasekhar, 1960; Irvine  
216 1964; Ivanov and Gutshabash 1974; van de Hulst, 1980, 2012; Ishimaru, 1999; Thomas and  
217 Stamnes, 2002; Davis and Marshak, 2002; Kokhanovsky et al., 2003; Marshak and Davis, 2005;  
218 Pandey et al., 2012; and etc.). In this study, we ~~are trying to~~ develop an analytic radiative  
219 transfer equation to analyze the radiative transfer at oxygen A and B bands. Through solving the  
220 analytic equation, we can retrieve the CTP information directly. The theory of CTP retrieval is  
221 similar for EPIC oxygen A-band and B-band observation. Here we use oxygen A-band as an  
222 example to study the radiative transfer model. For oxygen A-band, photon path length  
223 distribution is capable of describing vital information related to a variety of cloud and  
224 atmospheric characteristics.

$$225 \quad I_v(\mu, \varphi; \mu_0, \varphi_0) = I_0(\mu, \varphi; \mu_0, \varphi_0) \int_0^{\infty} p(l, \mu, \varphi; \mu_0, \varphi_0) e^{-\kappa_v l} dl \quad (1)$$

226 Where,  $p(l)$  is photon path length distribution,  $\kappa_v$  is the gaseous absorption coefficient at wave  
227 number  $v$ ,  $\mu = \cos(\theta)$ ,  $\mu_0 = \cos(\theta_0)$ ,  $(\theta, \varphi; \theta_0, \varphi_0)$  are zenith and azimuth angles for solar and

228 sensor view respectively,  $I_0$  and  $I_v$  are incident solar radiation and sensor measured solar radiation,  
 229 respectively.

230 When clouds exist, the incident solar radiation is reflected to ~~outer space~~ TOA in three  
 231 primary ways. First, incident solar radiation is reflected by cloud top layer directly as a result of  
 232 single scattering. Second, the incident solar radiation will penetrate into the cloud and be  
 233 reflected back to TOA through cloud top via multiple scattering. Third, the incident solar  
 234 radiation will pass through the cloud and arrive at the surface, after that it is reflected back into  
 235 the cloud and finally scattered back to TOA through the cloud top. Due to the position of the  
 236 EPIC instrument and the long distance between EPIC and Earth, we can consider that solar  
 237 zenith angle and sensor view angle are nearly reverse. At oxygen A-band, the reflected solar  
 238 radiation will be reduced due to oxygen absorption depending on photon path length  
 239 distributions. Absorption is negligible in oxygen A-band's reference band. ~~For solar radiation at~~  
 240 ~~oxygen-Oxygen~~ A-band and its reference band, ~~they~~ are also attenuated by airmass and aerosol  
 241 ~~that located above or below cloud~~ through Rayleigh scattering and aerosol extinction. In the  
 242 standard atmospheric model, the optical depth of Rayleigh scattering ( $\tau_{Ray}$ ) at oxygen A-band  
 243 (B-band) and its reference band is 0.026 (0.040) and 0.024 (0.042), respectively (Bodhaine et al.,  
 244 1999). The absolute difference of Rayleigh scattering optical depth ( $\Delta\tau_{Ray} = \tau_{Ray}^{In-band} - \tau_{Ray}^{Ref}$ )  
 245 between them is within 0.002. Compared to Rayleigh scattering, the difference of background  
 246 aerosol optical depth ( $\Delta\tau_{Aer}$ ) between ~~in-band~~ absorbing and reference bands is smaller, within  
 247 0.0005. ~~However~~ Therefore, their attenuations from Rayleigh scattering and aerosol extinction at  
 248 EPIC oxygen absorption and its reference band are close to each other. Thus, ~~we can~~ when we  
 249 use the ratio of EPIC measured reflectance at oxygen A-band and its reference band to derive the  
 250 photon path length distribution and retrieve cloud information such as CTP, the impact of  
 251 Rayleigh scattering and aerosol extinction can be simplified in the analytic transfer ~~inverse~~  
 252 model. ~~and then retrieve cloud information such as CTP.~~

253 To simplify the analytic transfer inverse model for EPIC observations, we made a series  
 254 of assumptions, e.g., isotropic component, a plane-parallel homogenous cloud assumption with  
 255 quasi-Lambertian reflecting surfaces, ~~and etc.~~ These assumptions have been widely used in  
 256 radiative transfer calculation for cloud studies. In this model,  $\mu$  and  $\mu_0$  are the same as in  
 257 Equation-Eq. (1),  $\varphi$  is the relative azimuth angle between solar-Sun and satellite sensors;  $A_{surf}$  is the  
 258 surface albedo;  $\tau_{O_2}^{Top}$ ,  $\tau_{O_2}^{Base}$ , and  $\tau_{O_2}^{Surface}$  are oxygen A-band absorption optical depth from  
 259 TOA to cloud top layer, cloud bottom layer, and surface, respectively;  $\Delta\tau_{O_2}^{Above-Clid}$ ,  
 260  $\Delta\tau_{O_2}^{In-Clid}$  and  $\Delta\tau_{O_2}^{Below-Clid}$  are layered oxygen A-band absorption optical depth above cloud, in  
 261 cloud, and below-cloud, respectively; functions  $f$  mean their contribution to the ratio of  
 262 measured reflectance at oxygen A-band ( $R_A$ ) and reference band ( $R_f$ ). The detailed analysis of  
 263 EPIC analytic transfer inverse model is shown as follows:

264 (1) **Above Cloud:** the reflected solar radiation is determined by the oxygen absorption optical  
 265 depth above the cloud and air mass directly.

$$\begin{aligned}
 266 \quad f(\Delta\tau_{O_2}^{Above-Clid}, \mu_0, \mu, \varphi) &= f(\Delta\tau_{O_2}^{Above-Clid})f(\mu_0, \mu, \varphi) \\
 267 \quad &= a_0 \tau_{O_2}^{Top} \left( \frac{1}{\mu} + \frac{1}{\mu_0} \right) \quad (2)
 \end{aligned}$$

268 [Here,  \$a\_0\$  is a weight coefficient.](#)

269 (2) **Within Cloud:** the reflected solar radiation is not only determined by oxygen absorption  
 270 optical depth above cloud and in-cloud, but also by penetration related factors, e.g., [cloud optical](#)  
 271 [depthCOD](#). Due to photon penetration, oxygen parameter  $\tau_{O_2}^{Top}$  influences the enhanced path  
 272 length absorption:

$$273 \quad \Delta\tau_{O_2}^{In-Cloud} = \tau_{O_2}^{Base} - \tau_{O_2}^{Top} \quad (3)$$

274 Equivalence theorem (Irvine, 1964; Ivanov and Gutshabash, 1974; van de Hulst 1980) is used to  
 275 separate absorption from scattering:

$$276 \quad f(\tau_{O_2}^{Top}, \Delta\tau_{O_2}^{In-Cloud}, \mu_0, \mu, \varphi) = f(\tau_{O_2}^{Top}, \Delta\tau_{O_2}^{In-Cloud})f(\mu_0, \mu, \varphi) \\ 277 \quad = f(\tau_{O_2}^{Top})f_1(\mu_0, \mu, \varphi) + f(\Delta\tau_{O_2}^{In-Cloud})f_2(\mu_0, \mu, \varphi) \quad (4)$$

278  $f(\tau_{O_2}^{Top})$  is determined by two absorption dependences: strong ( $\sim \sqrt{\tau_{O_2}^{Top}}$ ) and weak ( $\sim \tau_{O_2}^{Top}$ ).

$$279 \quad f(\tau_{O_2}^{Top}) = a_1 \sqrt{\tau_{O_2}^{Top}} + b_1(\tau_{O_2}^{Top}) \quad (5)$$

280 Based on asymptotic approximation (Kokhanovsky *et al.*, 2003; Pandey *et al.*, 2012), the  
 281 reflection of a cloud without considering below cloud interaction is given by [Equation-Eq. \(6\)](#):

$$282 \quad R(\tau, \mu, \mu_0, T) = R_0^\infty(\tau, \mu, \mu_0) - TK(\mu)K(\mu_0) \\ 283 \quad = R_0^\infty(\tau, f_1(\mu, \mu_0)) - Tf_2(\mu, \mu_0) \quad (6)$$

284 Here,  $R_0^\infty$  is the reflectance of a semi-infinite cloud,  $K(\mu)$  is the escape function of  $\mu$ ,  $T$  is global  
 285 transmittance of a cloud.  $T$  can be estimated by [Equation-Eq. \(7\)](#), with the cloud optical  
 286 thickness  $\tau_{cloud}$ , the asymmetry parameter  $g$ , and [a numerical constant  \$\alpha = 1.07\$ -a numerical](#)  
 287 [constant](#).

$$288 \quad T = \frac{1}{0.75\tau_{cloud}(1-g)+\alpha} \quad (7)$$

289  $f_1$  and  $f_2$  functions have a quadratic form as follows:

$$290 \quad f_{i-1} = a_i T + b_i(\mu + \mu_0) + c_i T(\mu + \mu_0) + d_i \mu \mu_0, i = 2,3 \quad (8)$$

291 Combining [Equations \(4\), \(5\) and \(8\)](#), we can get the [equation-Eq. \(9\)](#):

$$292 \quad f(\tau_{O_2}^{Top}, \Delta\tau_{O_2}^{In-Cloud}, \mu_0, \mu, \varphi) = \left( a_1 \sqrt{\tau_{O_2}^{Top}} + b_1(\tau_{O_2}^{Top}) \right) (a_2 T + b_2(\mu + \mu_0) + c_2 T(\mu + \mu_0) + d_2 \mu \mu_0) \\ 293 \quad + \Delta\tau_{O_2}^{In-Cloud} (a_3 T + b_3(\mu + \mu_0) + c_3 T(\mu + \mu_0) + d_3 \mu \mu_0) \quad (9)$$

295 (3) **Below Cloud:** The equivalence theorem used for below cloud is similar to within cloud  
 296 (Kokhanovsky *et al.*, 2003; Pandey *et al.*, 2012).

$$297 \quad f(\Delta\tau_{O_2}^{Below-Cloud}, \mu_0, \mu, \varphi) = T \tau_{O_2}^{Surface} \frac{A_{Surf}}{1+(e_4 * T + f_4) * A_{Surf}} \\ 298 \quad * (a_4 T + b_4(\mu + \mu_0) + c_4 T(\mu + \mu_0) + d_4 \mu \mu_0) \quad (10)$$

299

Combining Equations (2), (9) and (10), we can get the total EPIC analytic transfer equation as follows

$$-\log\left(\frac{R_A}{R_f}\right) = f(\Delta\tau_{O_2}^{Above-Cloud}, \mu_0, \mu, \varphi) + f(\tau_{O_2}^{Top}, \Delta\tau_{O_2}^{Cloud}, \mu_0, \mu, \varphi) + f(\Delta\tau_{O_2}^{Below-Cloud}, \mu_0, \mu, \varphi) + \Delta\tau_{BG} \left(\frac{1}{\mu} + \frac{1}{\mu_0}\right) \quad (11)$$

In Equation (11),  $\Delta\tau_{BG}$  represents the sum of optical depth difference of background extinction (i.e., Rayleigh scattering  $\Delta\tau_{Ray}$ , aerosol extinction  $\Delta\tau_{Aer}$ , and O3  $\Delta\tau_{O_3}$ ) between oxygen in-band and reference band, as shown in Equation (12).

$$\Delta\tau_{BG} = \Delta\tau_{Ray} + \Delta\tau_{Aer} + \Delta\tau_{O_3} \quad (12)$$

As stated in the previous subsection, in the standard atmospheric model with background aerosol loading, ( $\Delta\tau_{Ray}$ ,  $\Delta\tau_{Aer}$ ,  $\Delta\tau_{O_3}$ ) is approximately (0.002, 0.0005, -0.0005) and (-0.002, -0.0005, -0.002) respectively at oxygen A and B bands, thus  $\Delta\tau_{BG}$  is approximately 0.002 and -0.0045 respectively at these two bands.

In this total analytic equation, there are 16-17 coefficients ( $a_0, a_1, b_1, a_2, \dots, d_4, e_4, f_4$ ), which can be calculated through nonlinear regression algorithm according to a series of simulated values for different atmospheric conditions. Based on Equation-Eq. (11), we can finally obtain a

quadratic equation,  $\mathbf{A} \sqrt{\tau_{O_2}^{Top}}^2 + \mathbf{B} \sqrt{\tau_{O_2}^{Top}} + \mathbf{C} = \mathbf{0}$ , where the parameters A, B and C (not shown here) can be derived from Equation-Eq. (11) directly, as shown in Equation (13).

$$A = a_0 \left(\frac{1}{\mu} + \frac{1}{\mu_0}\right) + b_1(a_2 T + b_2(\mu + \mu_0) + c_2 T(\mu + \mu_0) + d_2 \mu \mu_0) \quad (13.1)$$

$$B = a_1(a_2 T + b_2(\mu + \mu_0) + c_2 T(\mu + \mu_0) + d_2 \mu \mu_0) \quad (13.2)$$

$$C = -\log\left(\frac{R_A}{R_f}\right) - \Delta\tau_{BG} \left(\frac{1}{\mu} + \frac{1}{\mu_0}\right) - \Delta\tau_{O_2}^{In-Cloud} (a_3 T + b_3(\mu + \mu_0) + c_3 T(\mu + \mu_0) + d_3 \mu \mu_0) - T \tau_{O_2}^{Surface} \frac{A_{Surf}}{1+(e_4 T + f_4) A_{Surf}} (a_4 T + b_4(\mu + \mu_0) + c_4 T(\mu + \mu_0) + d_4 \mu \mu_0) \quad (13.3)$$

When these parameters (i.e., A, B and C) are obtained from EPIC observation data and other data source, we can easily solve the quadratic equation to retrieve cloud top O2 absorption depth, and then CTP.

## 2.3 Detailed retrieval algorithm

As previously stated, in method 2, the analytic EPIC equation (i.e., Equation-Eq. (11)) is key for the CTP retrieval. To derive the coefficients of Equation-Eq. (11), a series of model simulations for various atmospheric conditions are needed. Thus, developing a radiative transfer model to simulate the EPIC measurements at A- and B-bands and their reference bands is the first thing we need to complete.

### 42.3.1 Oxygen A- and B-band absorption coefficients calculation

To simulate the EPIC measurements, one of the most important steps is calculating oxygen absorption coefficients at oxygen A-band and B-band. In this step, the latest-HITRAN

333 [2016](#) database ([Gordon et al., 2017](#)) is used to provide the absorption parameters, and the  
 334 LBLRTM package ([Clough et al., 2005](#)) is used to calculate oxygen absorption coefficients layer  
 335 by layer. In our algorithm, the whole Earth atmosphere is divided by 63 layers.

336 Since oxygen absorption coefficients are pressure (or pressure-squared) and temperature  
 337 dependent, and the line [shapes \( \$k\_i\$ \) of oxygen A- and B-bands](#) are well fitted as Lorentzian in the  
 338 lower atmosphere, the relationship can be written as follows:

$$339 \quad k_i = \frac{S_i}{\pi} \frac{\alpha_i}{(v-v_i)^2 + \alpha_i^2} \quad (4214)$$

$$340 \quad \alpha_i = \alpha_i^0 \frac{P}{P_0} \left(\frac{T_0}{T}\right)^{\frac{1}{2}}, \quad S_i = S(T_0) \frac{T_0}{T} \exp \left[1.439E \left(\frac{1}{T_0} - \frac{1}{T}\right)\right] \quad (4315)$$

341 Where  $S_i$  is the line intensity,  $v_i$  and  $\alpha_i$  are the line center wave number and half width,  
 342 respectively;  $P$  and  $T_0$  are standard atmospheric pressure and temperature, respectively.

343 ~~An unfortunate result of this is that cloud levels at a given pressure-weighted oxygen~~  
 344 ~~absorption depth~~In the simulation of EPIC measurements, the atmospheric layer at a given layer-  
 345 ~~average pressure~~ can have drastically different ~~temperature heights~~ depending on the  
 346 atmospheric profile in use. ~~We have used~~To ensure the accuracy of simulation, we need to use  
 347 the LBLRTM package to calculate oxygen ~~absorption coefficients~~parameters for each  
 348 pressure/temperature profile; ~~which is~~ a time-consuming process. Our goal has been to find a  
 349 simple and fast ~~method to calculate oxygen absorption coefficient~~conversion function from  
 350 ~~pressure to altitude~~ for different atmospheric profiles. ~~Based on the study of Chou and Kouvaris~~  
 351 ~~(1986), Min et al. (2014) proposed a fast method to calculate oxygen absorption optical depth for~~  
 352 ~~any given atmosphere by Using-using~~ a polynomial fitting function, ~~as shown in Equation. 16. ;~~  
 353 ~~fitting coefficients can be determined for oxygen absorption and applied to any given atmosphere~~  
 354 ~~(Min et al., 2014; Chou and Kouvaris, 1986).~~

$$355 \quad \ln(A_{vLM}) = [a_0(v, P) + a_1(v, P) \times (T_{LM} - T_{mL}) + a_2(v, P) \times (T_{LM} - T_{mL})^2] \times \rho_{O_2} \quad (4416)$$

356 Where  $A_{vLM}$  is optical depths for layer L, spectral point v, and atmosphere model M;  $\rho_{O_2}$  is  
 357 molecular column density ( $\frac{\text{molecules}}{\text{cm}^2} \times 10^{-23}$ );  $T_{LM}$  is the average temperature for layer L for a  
 358 given atmosphere; and  $T_{mL}$  is average temperature over all [six typical geographic-seasonal model](#)  
 359 atmospheres (M1 to M6, [i.e., tropical model, mid-latitude summer model, mid-latitude winter](#)  
 360 [model, subarctic summer model, subarctic winter model, and the U.S. Standard \(1976\) model](#))  
 361 for layer L. ~~To derive the coefficients  $a_0$ ,  $a_1$ , and  $a_2$ , we first~~by ~~calculated oxygen optical depth~~  
 362 ~~coefficients for all typical atmospheres (M1 to M6) by using LBLRTM package, and then~~  
 363 ~~selected three of them (e.g., M1, M5, and M6) to calculate the polynomial fitting coefficients.~~  
 364 ~~This method has been successfully used by Min et al. (2014) to simulate the high resolution~~  
 365 ~~oxygen A-band measurements.~~

366

### 367 **42.3.2 Fast radiative transfer model for simulating high-resolution oxygen A- and B-bands**

368 ~~At oxygen A and B absorption bands, there are lots of absorption lines, therefore w~~We  
 369 cannot simply calculate narrowband mean optical depth and then calculate the radiation for  
 370 various atmospheric conditions when simulating EPIC narrowband measurements. The correct  
 371 way is described as follows: firstly, simulate the solar radiation spectrum  $S(k(\lambda))$  under specific

372 atmospheric conditions, then integrate the spectrum with EPIC narrowband filter  $R(k(\lambda))$  to  
 373 obtain simulated narrowband measurements ([Equation-Eq. 15\(17\)](#)).

$$374 \quad R(\lambda) = \int S(k(\lambda))R(k(\lambda))d\lambda \neq R(\overline{k(\lambda)}) \quad (4517)$$

375 With the high spectrum resolution oxygen absorption coefficient data, we can simulate the  
 376 high resolution upward diffuse oxygen A-band or B-band spectrum through DISORT code  
 377 (Stamnes et al., 1988) for any given atmospheric condition, which has various surface albedo,  
 378 SZA, [cloud optical depthCOD](#), [cloud top heightCTH](#) ([pressureCTP](#)), and cloud geometric  
 379 (pressure) thickness. However, due to the high spectrum resolution, it is very time-consuming  
 380 when performing line by line (LBL) calculations. Thus, developing a fast radiative transfer  
 381 model for simulating high resolution oxygen A-band and B-band spectrum is necessary.

382 In this project, the double- $k$  approach is used to develop a fast radiative transfer model for  
 383 oxygen A-band and B-band respectively. [Min and Harrison 2004; Duan et al, 2005] proposed a  
 384 fast radiative transfer model. In their approach, the radiation from absorption and scattering  
 385 processes of cloud and aerosol are split into the single- and multiple-scattering components: The  
 386 single scattering component is computed line-by-line (LBL), while multiple scattering (second  
 387 order and higher) radiance is approximated.

$$388 \quad I = I^{ss}(\lambda) + I^{ms}(\lambda)$$

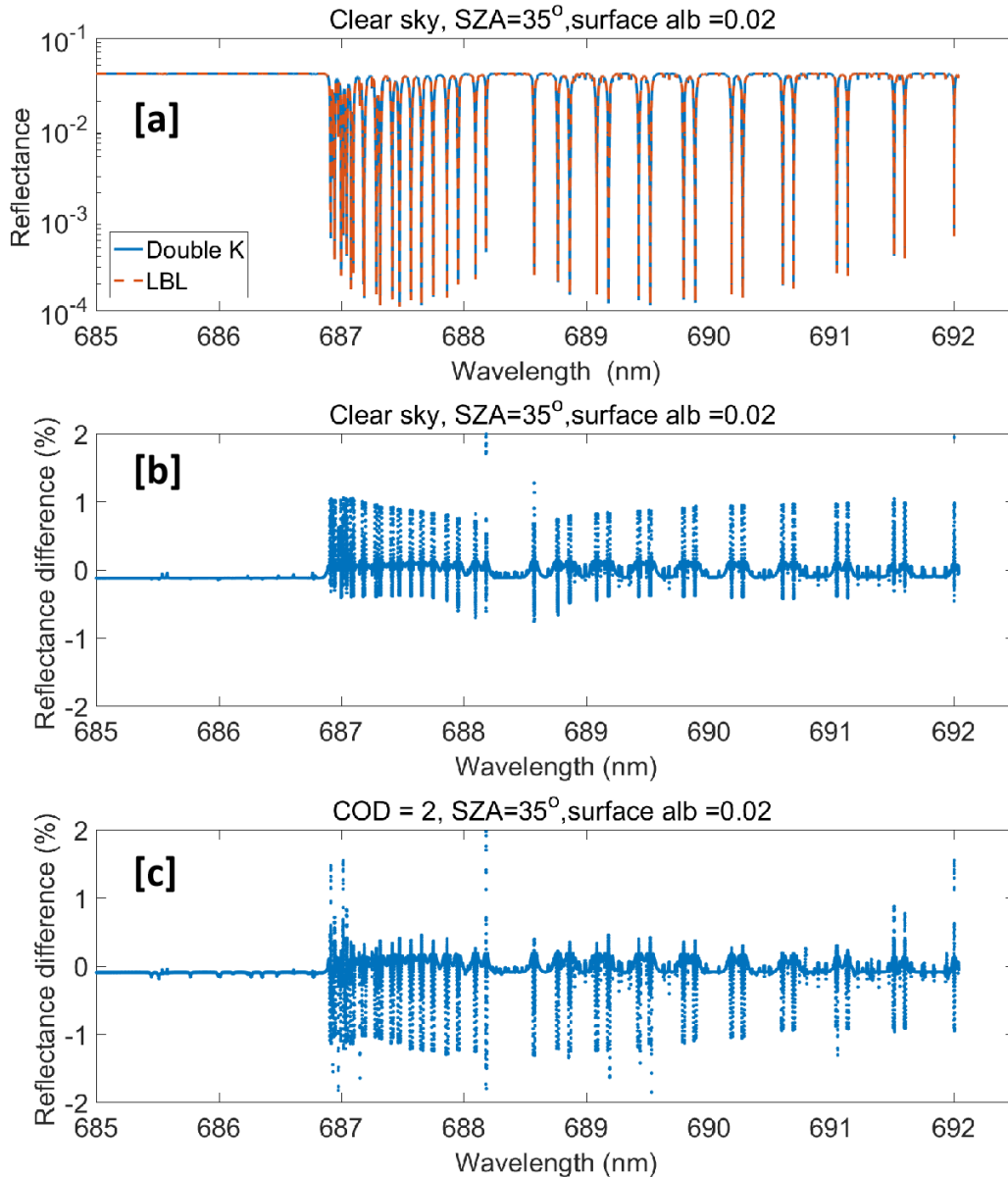
$$389 \quad \approx I^{ss}[Z^h(p, \epsilon T), P^h, \lambda] + I^{ms}[Z^h(p, \epsilon T), P^h, \lambda]$$

$$390 \quad \approx I^{ss}[Z^h(p, \epsilon T), P^h, \lambda] + I^{ms}[Z^l(p, \epsilon T), P^l, \lambda]$$

$$391 \quad \approx I^{ss}[Z^h(p, \epsilon T), P^h, \lambda] + I^{ms}\{F[Z^l(p, \epsilon T), P^l, k(\lambda_i)]\} \quad (4618)$$

392 [Equation-Eq. 16\(18\)](#) is from [Equation-Eq. \(1\)](#) in Duan et al. (2005):  $ss$  and  $ms$  mean single and  
 393 multiple scattering, respectively.  $Z$  is the optical properties of the atmosphere as a function of  
 394 pressure  $p$  and temperature  $T$ , with  $P$  being the phase function of that layer.  $h$  and  $l$  represent  
 395 higher and lower number of layers and streams, respectively.  $F$  is the transform function between  
 396 wave number space and  $k$  space, defined from a finite set of  $k(\lambda_i)$ .

397 The application of Double- $k$  approach in oxygen A-band has been presented in detail in  
 398 Duan et al. 2005. Here we take oxygen B-band as an example. The detailed fast radiative transfer  
 399 model for simulating high-resolution oxygen B-band is as follows: The first order scattering  
 400 radiance is calculated accurately by using a higher number of layers and streams for all required  
 401 wavenumber grid points. The multiple-scattering component is extrapolated and/or interpolated  
 402 from a finite set of calculations in the space of two integrated gaseous absorption optical depths  
 403 to the wavenumber grids: a double- $k$  approach. The double- $k$  approach substantially reduces the  
 404 error due to the uncorrelated nature of overlapping absorption lines. More importantly, these  
 405 finite multiple-scattering radiances at specific  $k$  values are computed with a reduced number of  
 406 layers and/or streams in the forward radiative transfer model. To simulate an oxygen B-band  
 407 spectrum with high accuracy, 33  $k$  values and 99 calculations of radiative transfer are chosen in  
 408 our program. This results in around a hundred-fold time reduction with respect to the standard  
 409 forward radiative transfer calculation.



410

411 **Figure 2.** [a] High resolution reflectance at EPIC O2 B-Band simulated by fast radiative model  
 412 (double-k) and benchmark (LBL); Difference between simulated reflectance by double-k and  
 413 LBL for a clear sky case [b] and a [thin liquid water](#) cloud case with COD=2 [c]. Here SZ=35°  
 414 and view angle =35°, surface albedo = 0.02, [aerosol optical depth = 0.08](#), and [reflectance](#)  
 415 [difference \(%\) = 100\\*\(\(double-k\) - LBL\)/LBL](#).

416 As shown in Figure 2, under clear sky and thin [liquid water](#) cloud situations, the  
 417 simulated high resolution upward diffuse oxygen B-band spectra from LBL calculation and  
 418 double-k approach are compared. The spectrum difference between LBL calculation and double-  
 419 k approach is very small **and hard to tell directly** (Figure 2a). Under both situations, most of the  
 420 relative difference between these two methods are under 0.5%. The obvious relative difference  
 421 (>1%) occurs only in the wavelength range with high absorption optical depth, which has little  
 422 contribution to the integrated solar radiation. Therefore, for the simulated narrowband

423 measurements at EPIC oxygen B-band, the relative difference between LBL and double-k  
 424 approach is much smaller than that of the high resolution spectrum, which is less than 0.1% for  
 425 ~~both~~ clear day. Compared to clear sky situation, the relative difference for ~~and~~ cloud situations  
 426 can be bigger. As (shown in Table 1, the relative difference is -0.06% and -0.32% for typical  
 427 high level optical thin cloud and low-level thick cloud situations, respectively). For optically  
 428 thick cloud situations, the accuracy of the double k approach is similar to that of thin cloud  
 429 situations. The comparison of simulated narrowband measurement at EPIC oxygen A-band  
 430 channel (764 nm) is also shown in Table 1, the relative differences between LBL and double-k  
 431 approach are -0.06%, 0.21% and 0.23% for clear day, high level thin cloud and low level thick  
 432 cloud cases, respectively. In general, the accuracy of double-k approach for both oxygen A and B  
 433 absorption bands is high.

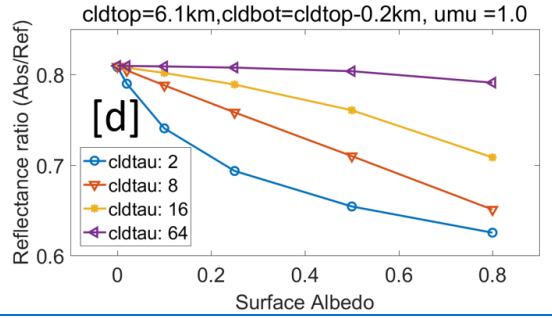
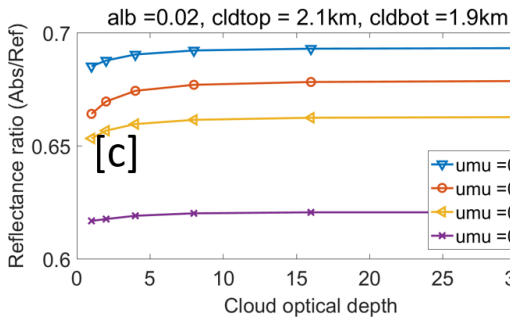
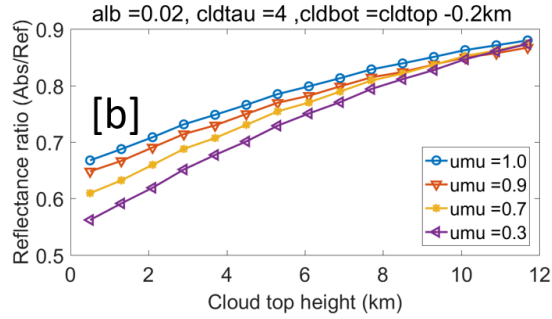
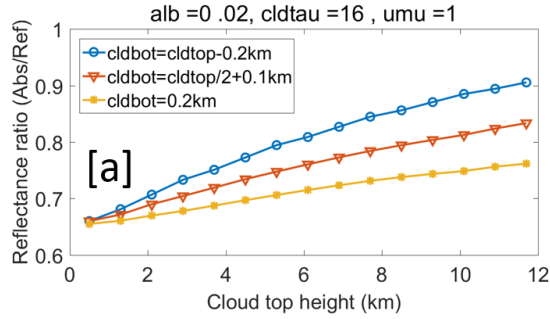
434 **Table 1.** Comparison of simulated narrowband measurement at EPIC A- and B-Band channels

Case	Line by line	Double k	Difference	
Clear day	0.026963	0.026985	+0.08%	
Thin Cloud	0.084046	0.084033	-0.02%	
Case (SZA=35, surface albedo =0.02)		Line by Line	Double k	Relative Difference
Clear Day	688 nm	0.026963	0.026985	+0.08%
	764 nm	0.013979	0.013970	-0.06%
Thin cloud (COD=2, 8.3- 8.5 km, liquid)	688 nm	0.098444	0.098131	-0.32%
	764 nm	0.071359	0.071507	+0.21%
Thick cloud (COD=16, 1.5- 2.9 km, liquid)	688 nm	0.396354	0.396117	-0.06%
	764 nm	0.233937	0.234485	+0.23%

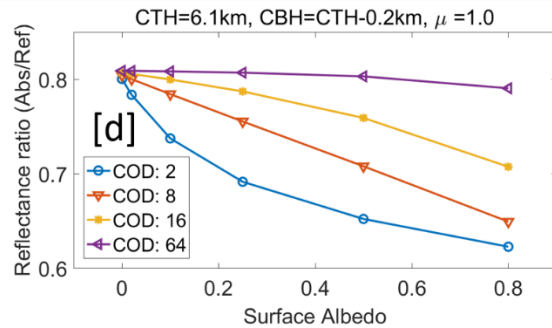
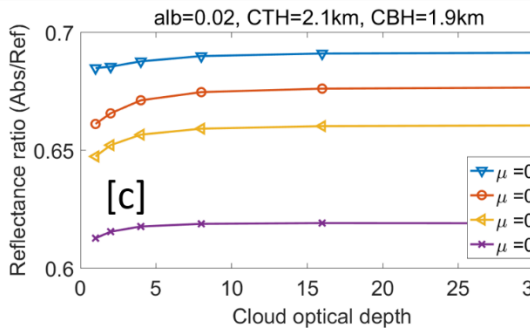
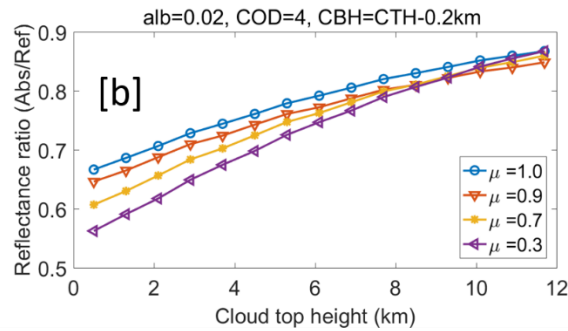
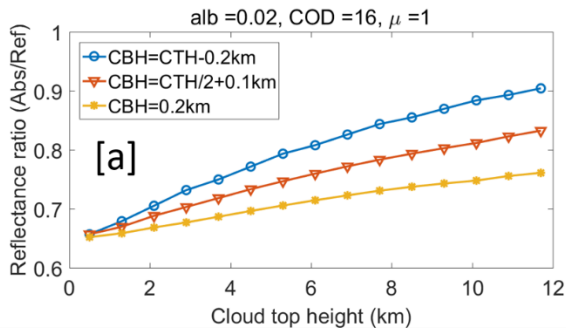
435

436 **42.3.3 Simulation of oxygen A- and B-bands for different atmospheric conditions**

437 Using the EPIC measurement simulation package, we made a series of simulations with  
 438 different settings for surface albedo, solar zenith angle, ~~cloud optical depth~~ COD, ~~CTH~~ cloud top  
 439 ~~height~~ (pressure CTP), and cloud geometric (pressure) thickness (or cloud bottom height). The  
 440 results of these simulations consist of a data table, which can be used not only to calculate the  
 441 coefficients for the analytic equation, but also to study the ~~sensibility~~ sensitivity of every  
 442 ~~variant~~ variable.



443

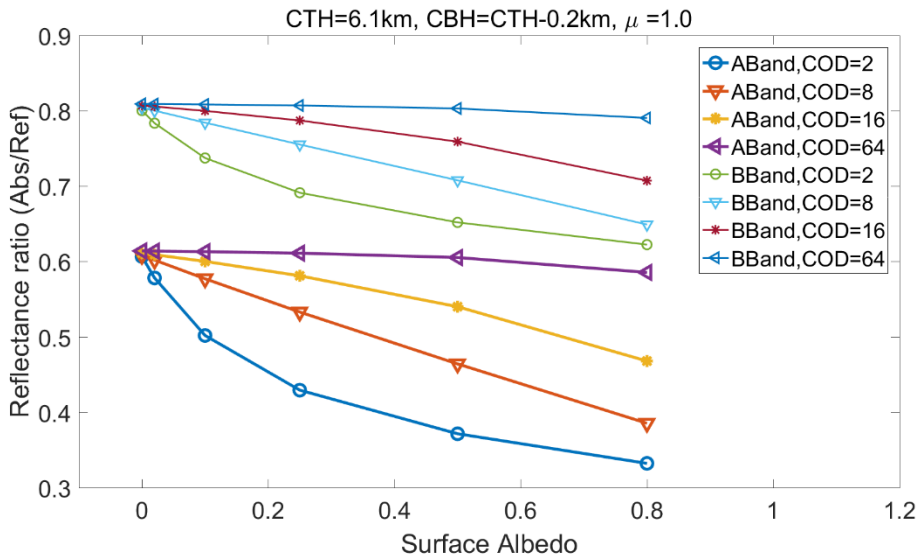


444

445 **Figure 3.** Ratio of simulated reflectance measurements for EPIC B-band to B-band reference  
 446 with different surface albedo ( $alb$ ), cloud optical depth  $COD$ ,  $\mu$  (cosine of solar zenith angle),  
 447 cloud top height ( $CTH$ ) and cloud bottom height ( $CBH$ ).

448 According to the previous theory study, the ratio of reflectance radiance (i.e., absorption  
 449 to the reference) at TOA is determined by the photon path length distribution at oxygen A/B  
 450 bands: the larger the mean photon path length, the stronger the absorption, and the smaller the  
 451 reflectance ratio. To make the figures easy to view and understand, we use cloud top and bottom  
 452 geometric height to represent  $CTP_{cloud\ top\ pressure}$  and thickness information in Figure 3. As  
 453 shown in Figure 3a, the ratio of upward diffuse radiance at oxygen B-band and its reference band

454 is sensitive to the cloud top height (pressure). The higher the [cloud top height](#) CTH, the larger the  
 455 ratio. At the same time, this ratio is affected by the cloud bottom height (or cloud geometric  
 456 thickness) when the other cloud parameters are fixed, the lower the cloud bottom (or the larger  
 457 the cloud geometric thickness), the smaller the ratio. It is consistent with the theory analysis: (1)  
 458 the higher the [cloud top height](#) CTH, the shorter the mean photon path length, and the weaker the  
 459 absorption; (2) when the [cloud optical depth](#) COD is given, larger cloud geometric thickness  
 460 means smaller cloud density, then the sunlight can penetrate deeper into the cloud, which results  
 461 in a longer mean photon path length. In Figure 3b, for clouds with given [cloud top height](#) CTH,  
 462 [cloud optical depth](#) COD and geometric thickness, the ratio decreases with the solar and view  
 463 angles. This ~~is easy to understand~~ can be understood as: the larger the solar and view angles, the  
 464 longer the mean photon pathlength, and the stronger the absorption. In Figure 3c, for clouds with  
 465 given [cloud top height](#) CTH and geometric thickness, when the [cloud optical depth](#) COD is small  
 466 (e.g., COD <5), the reflectance ratio increases with [cloud optical depth](#) COD. However, when  
 467 [cloud optical depth](#) COD is larger than 16, the effect of [cloud optical depth](#) COD is small. This is  
 468 because the larger the [cloud optical depth](#) COD, the shallower the sunlight penetration, and the  
 469 shorter the mean photon pathlength. In Figure 3d, for clouds with given [cloud optical depth](#) COD,  
 470 CTP, and geometric thickness, the ratio decreases with surface albedo. The smaller the [cloud](#)  
 471 [optical depth](#) COD, the stronger the impact of the surface albedo. This is because the [heavy-thick](#)  
 472 cloud prevents the incident sunlight from passing through it to reach the surface, and also  
 473 prevents the reflected light from going back to the TOA.



474  
 475 [Figure 4. Ratio of simulated reflectance measurements for EPIC A and B absorption band to](#)  
 476 [reference band with different surface albedo.](#)

477 For oxygen A-band, the ratio of upward diffuse at absorption and reference bands shows  
 478 similar characteristics as [for](#) oxygen B-band. Compared to oxygen B-band, under the same  
 479 atmospheric conditions, the oxygen absorption at A-band is stronger, and the ratio of A-band to  
 480 its reference band has smaller values [\(shown in Figure 4\)](#). [As stated previously, for land area that](#)  
 481 [covered with plants, the surface albedo may change substantially from oxygen B-band to A-band](#)  
 482 [due to the presence of the red edge. Therefore, accurate spectral data of surface albedo for CTP](#)  
 483 [retrieval is vitally important, especially for optically thin clouds.](#)

484

### 485 **3. Application and validation of the CTP retrieval method**

#### 486 **3.1 Case studies of cloud top pressure CTP retrieval**

487 The dataset of DSCOVR EPIC measurements at GMT 00:17:51 on July 25, 2016 is used for  
488 the case studies. The reflectance at oxygen A and B bands with related solar zenith and viewing  
489 angles are obtained from the EPIC level 1B data; COD information (retrieved from other EPIC  
490 channels) is obtained from EPIC level 2 data. The surface albedo data is obtained from Global  
491 Ozone Monitoring Experiment 2 (GOME-2) Surface Lambertian-equivalent reflectivity (LER)  
492 data. The detailed information of dataset is shown in the acknowledgements and dataset. To  
493 reduce the impact of the Earth surface, we selected the region located in spatial range of (S75° to  
494 N85°, W177° to W175°) for case studies, which is mainly covered by ocean. To constrain the  
495 influence of surface albedo and broken clouds, only pixels with total cloud covering (i.e., EPIC  
496 Cloud mask = 4), surface albedo less than 0.05, and liquid assumed COD larger than 3 are  
497 considered. In the selected region, around 10000 pixels are finally chosen for case studies.

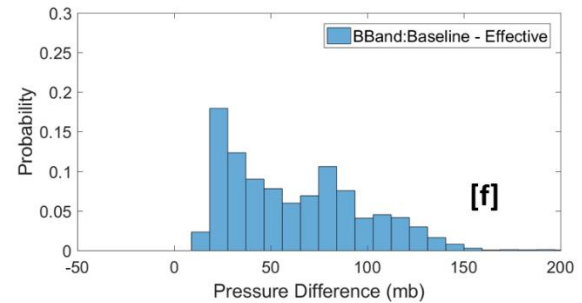
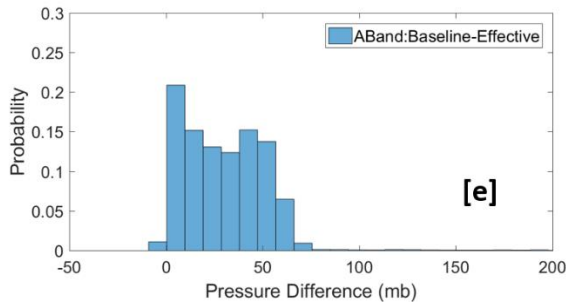
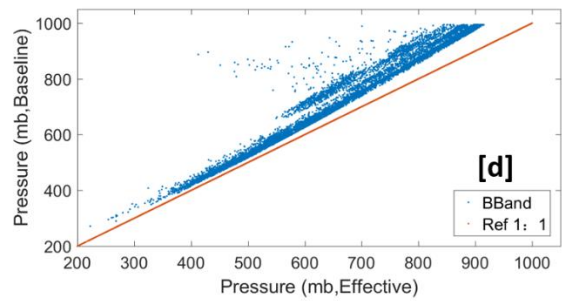
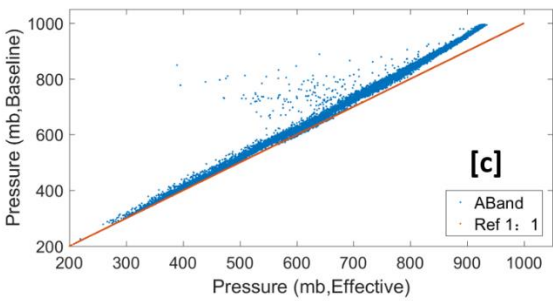
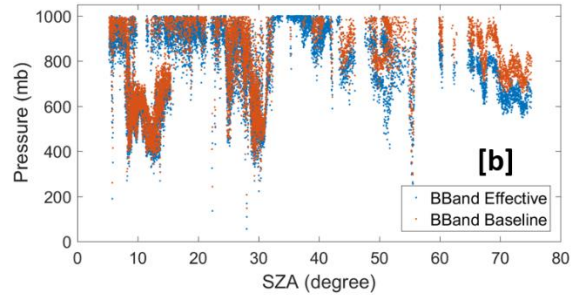
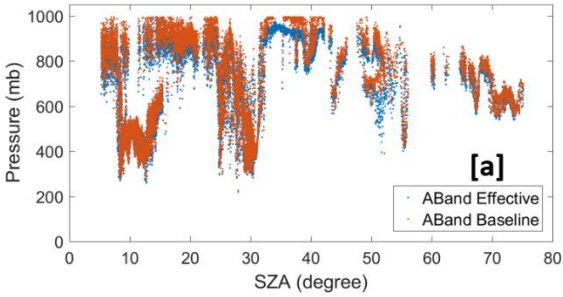
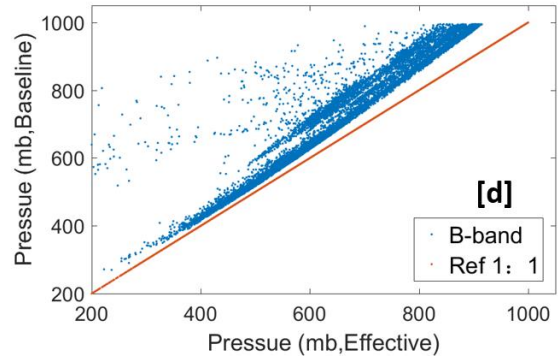
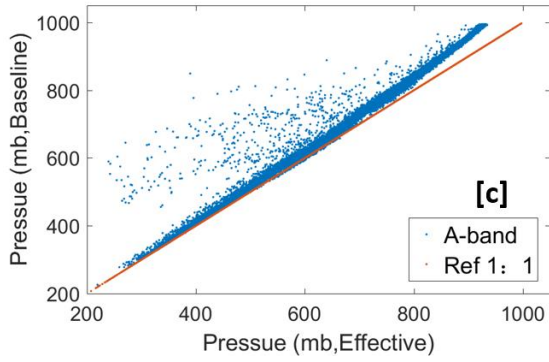
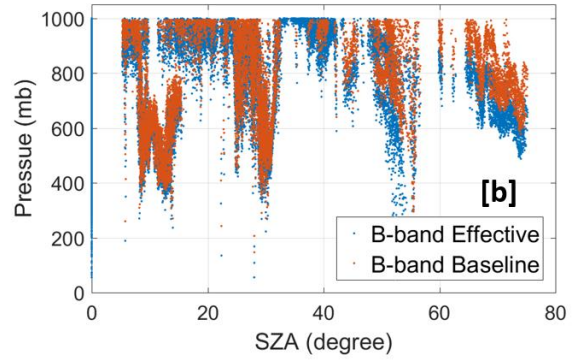
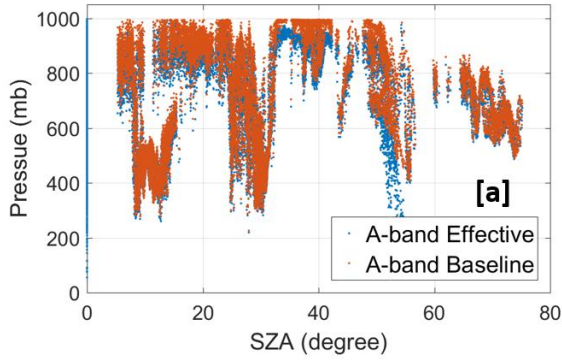
498 In our retrieval algorithm, we have two kinds of retrieval results: baseline CTP and retrieved  
499 CTP. The baseline CTP is used as a reference for the retrieved CTP. It is similar to the effective  
500 CTP in Yang et al., (20132019), which does not consider cloud penetration. The retrieved CTP is  
501 calculated by the analytic equation, which considers the in-cloud and below-cloud interaction.

502 During the baseline CTP calculation, the impact of penetration in-cloud is ~~ignorable~~ ignored,  
503 and the incident light that reached cloud top is assumed reflected back directly. As shown in  
504 Equation-Eq. 15(19), the baseline absorption optical depth  $\tau_{base}$  is derived from the ratio of  
505 upward diffuse at absorption bands and their reference bands directly. According to the model  
506 calculated oxygen A and B bands absorption optical depth profile at the specific solar zenith  
507 angle, the baseline CTP can be derived directly.

$$508 \tau_{base} = \log \left( -\frac{R_{abs}}{R_{ref}} \right) / \left( \frac{1}{\cos(\theta_{sza})} + \frac{1}{\cos(\theta_{view})} \right) \quad (4519)$$

509 As shown in Figure 45, the baseline CTP value at A-band is slightly higher than the  
510 effective CTP from NASA ASDC L2 data. But the baseline CTP value at B-band is substantially  
511 higher than the effective CTP from NASA ASDC L2 data. For both A-band and B-band, the  
512 difference between baseline CTP and effective CTP increases with the CTP. For low-level  
513 clouds, the mean differences of them are up to 60 mb and 100 mb at A-band and B-band,  
514 respectively. The difference may be mainly from the calculation of oxygen A and B bands  
515 absorption coefficients or the absorption optical depth profile.

516



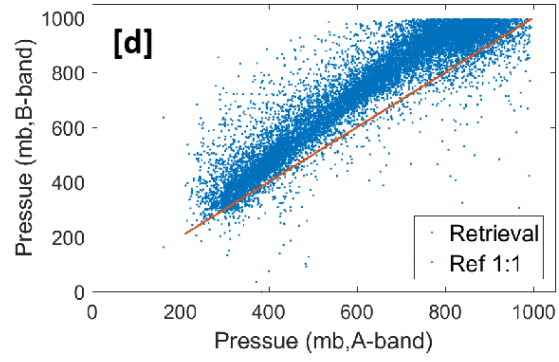
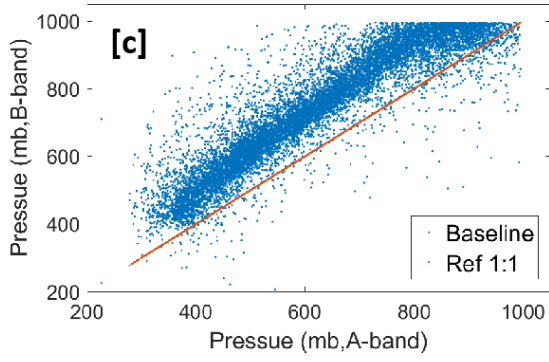
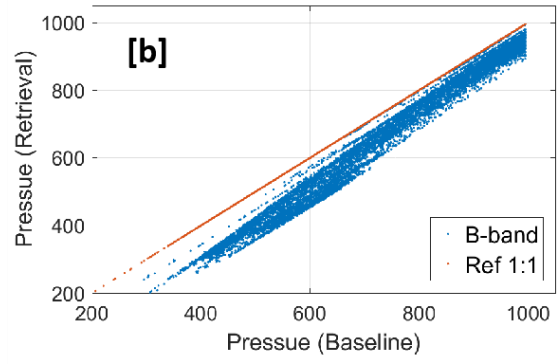
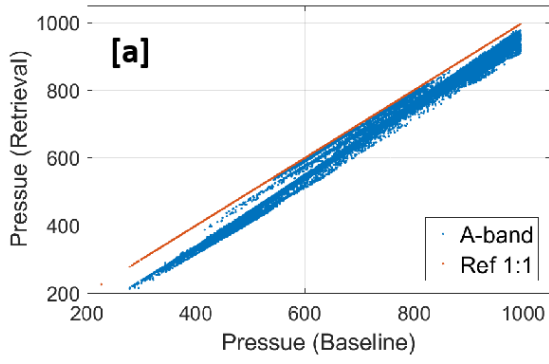
517

518

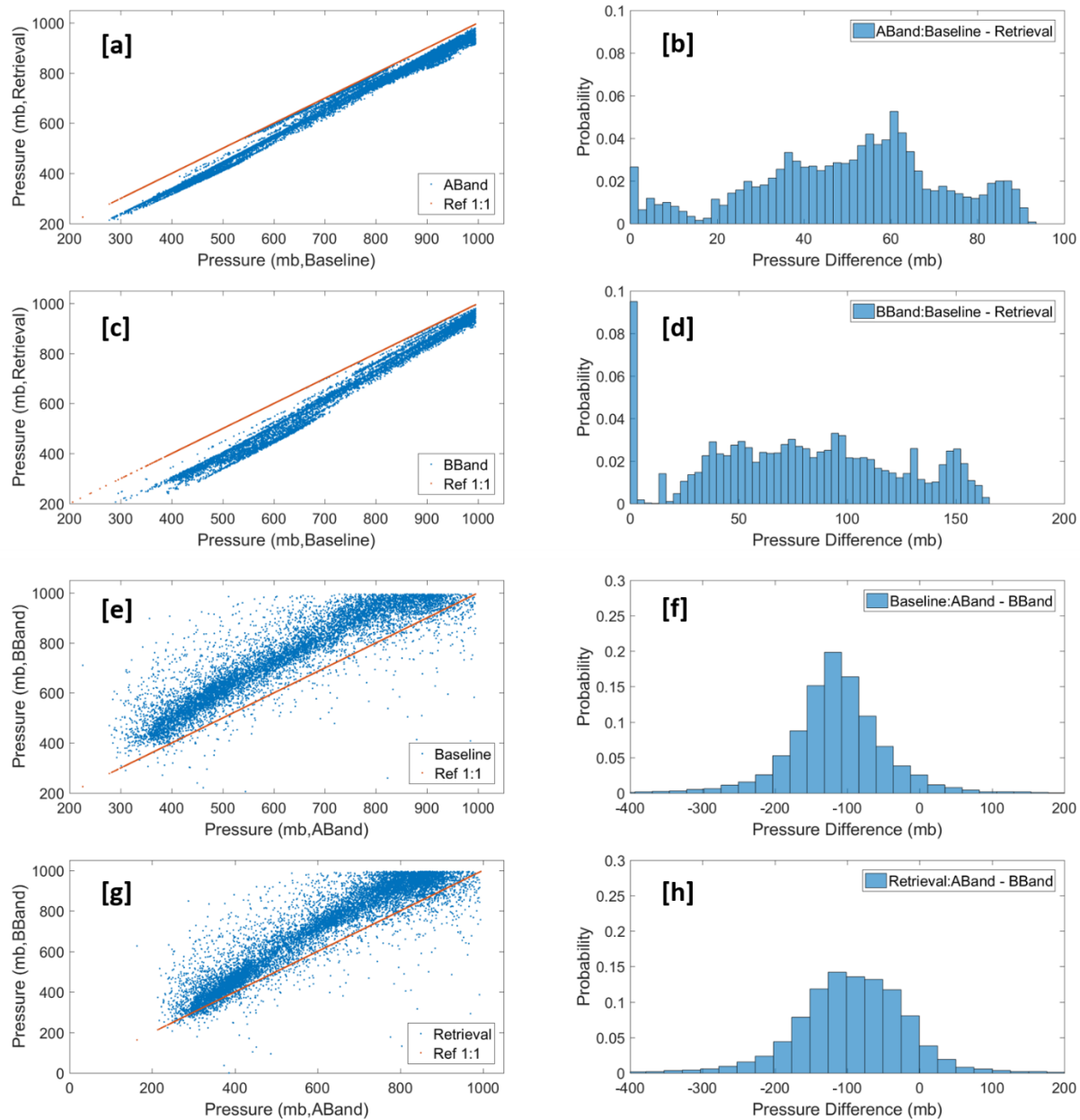
519 **Figure 45.** The comparison of effective CTP (reference from NASA ASDC data) and baseline  
520 values from our retrieval algorithm for EPIC A and B bands.

521 Based on the simulated reflectance ratio under different atmospheric conditions, we can  
522 calculate the coefficients for the analytic radiative transfer equations by using a nonlinear fitting  
523 algorithm. The coefficients for different SZA's are calculated individually to reduce the fitting  
524 error. Based on the calculated coefficients, we can retrieve the CTP with DISCOVER EPIC  
525 observation data at oxygen A and B bands.

526 During the CTP retrieval, with the exception of the previously mentioned analytic  
527 equation coefficients, we can get the surface albedo data from GOME, obtain reflectance data,  
528 solar zenith and view angles, ~~cloud optical depth~~COD, etc. from the NASA ASDC data file.  
529 Another very important step in the retrieval processing is the acquisition of cloud pressure  
530 thickness data, which has a substantial impact on the retrieval results. We currently use a  
531 statistical approach (i.e., cloud pressure thickness (mb) =  $2.5 * \text{cloud optical depth COD} + 2623$ ) to  
532 estimate the cloud pressure thickness based on ~~cloud optical depth~~COD. As shown in Figure 5a  
533 ~~6a-6d~~ and 5b, the retrieved CTP when considering cloud penetration is smaller than baseline  
534 CTP. For this case, the mean difference between baseline CTP and retrieved CTP for oxygen A-  
535 band and B-bands are around 57 mb and 85 mb, respectively, which is consistent with theoretical  
536 expectations. For clouds with a given CTP, the mean photon path length will increase  
537 substantially when considering cloud penetration ~~and interaction~~. A decrease in retrieved CTP  
538 will result in order to match the measurement ratio of absorption to reference. Compared to the  
539 O2 A-band, both baseline CTP and retrieved CTP for the O2 B-band are larger (Figure 5e-6e-  
540 ~~6h~~ and 5d). This is because the absorption of solar radiation in the O2 B-band is weaker than that  
541 of the O2 A-band, and the incident light at oxygen B-band can penetrate deeper into the cloud,  
542 allowing more light to pass through. The difference in retrieved CTP between B band and A  
543 band (approx. ~~101-93~~ mb with standard deviation of 83 mb) is generally reduced in comparison  
544 to baseline B band and A band (approx. ~~129-114~~ mb with standard deviation of 73 mb). This  
545 indicates, as expected, more photon penetration correction for B-band than A-band.



546



547  
 548 **Figure 56.** (a and b) The comparison of retrieved CTP and baseline values for EPIC A and B  
 549 bands; (c and d) the comparison of retrieved CTP and baseline values between EPIC A- and  
 550 B- bands.

551 We also used the LUT based method to do the retrieval for the same observation data,  
 552 because both methods share the same EPIC simulation package and the same simulated data  
 553 table, the results of which are similar.

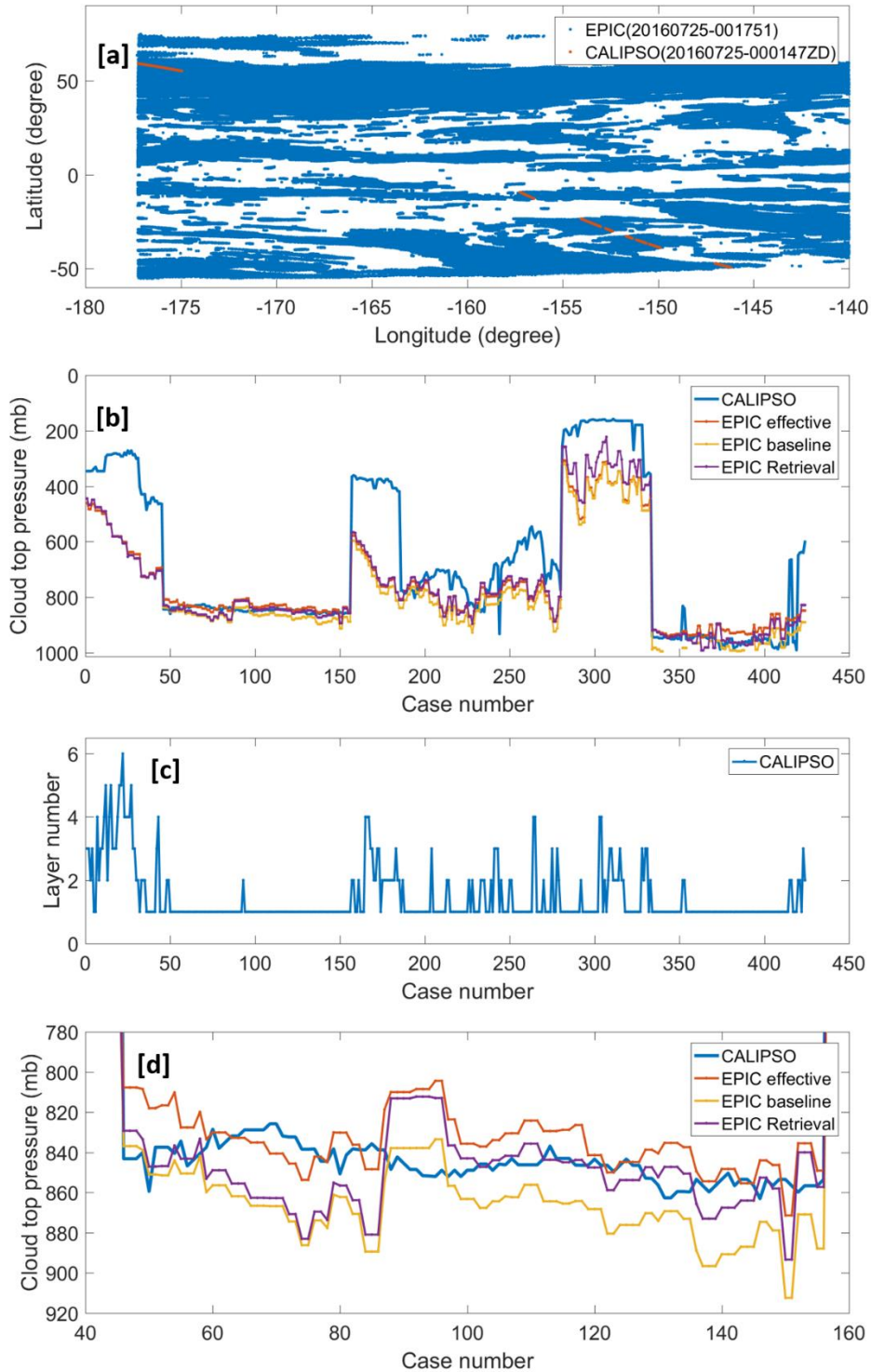
554

### 555 3.2 Validation of the retrieval method

556 To validate the analytic transfer inverse model method for CTP retrieval, we used another  
 557 independent measurement of CTP, i.e., cloud layer top pressure from Cloud-Aerosol Lidar and

558 Infrared Pathfinder Satellite Observations (CALIPSO, Vaughan et al., 2014) as a reference. For  
559 the previously stated case, i.e., DSCOVR EPIC measurements at GMT 00:17:51 on July 25,  
560 2016, we used the cloud layer data from CALIPSO IIR Version 4.2 Level 2 product with 5 km  
561 resolution at GMT 00:01:47 on July 25, 2016 as its reference to do validation. To constrain the  
562 error from spatial differences between different satellite measurements, we only chose the pixels  
563 of EPIC and CALIPSO measurements with a spatial distance of within 0.1° (degree of latitude or  
564 longitude) to make comparisons. For the EPIC measurements, the same as previously stated,  
565 only pixels with total cloud cover (i.e., EPIC Cloud mask = 4), surface albedo less than 0.05, and  
566 liquid assumed COD larger than 3 are considered. As shown in Figure 7a, there are a series of  
567 pixels (around 400 cases) from EPIC and CALISPO measurements can be used for the validation  
568 analysis. For the convenience of reading, we perform the analyses by using the case number as x  
569 axis. Figure 7b shows the comparisons of cloud layer top pressure from CALIPSO and different  
570 CTPs (i.e., effective CTP, baseline CTP, and retrieved CTP) from EPIC measurements. Figure  
571 7c shows the cloud layer number measured by CALIPSO. According to Figures 7b and 7c, we  
572 can get some results: under single layer cloud situations, the CTPs derived from EPIC  
573 measurements are close to the CTP from CALISPO; under multi-layer cloud situations, the CTP  
574 derived from EPIC measurements are larger than the CTP from CALISPO. Figure 7d shows the  
575 expanded view of the Figure 7b for some cases under single layer cloud situations. For these  
576 single layer cloud cases (with case number 46 ~ 156), the mean values of CTP of CALIPSO,  
577 EPIC effective, EPIC baseline and EPIC retrieval are 846, 834, 866 and 850 mb, respectively.  
578 Compared to the CTP from CALIPSO measurements , the EPIC effective and baseline CTPs are  
579 12 mb smaller or 20 mb larger, respectively; the EPIC retrieval with consideration of photon  
580 penetration is only 4 mb larger. This shows that our method for the CTP retrieval is valid and  
581 accurate under single layer cloud situations with COD > 3 and low surface albedo. Under multi-  
582 level cloud situations, the high-level clouds are often thin clouds, which can be detected by  
583 CALIPSO but hard to derive by our retrieval method. It is because the EPIC retrieved CTP  
584 mainly shows the pressure of cloud layer that reflects the major part of incident sun light.

585



586

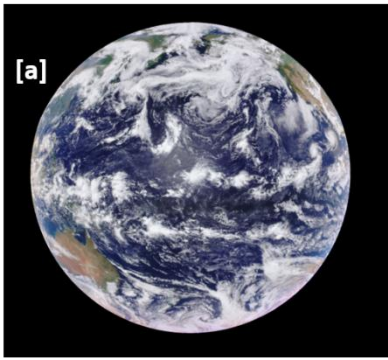
587 Figure 7. (a) The geolocation match of EPIC measurement at GMT 00:17:51 and CALIPSO  
 588 measurement at GMT 00:01:47 on July 25, 2016; (b) the comparisons of cloud layer top pressure  
 589 from CALIPSO measurements and the CTPs derived from EPIC measurements; (c) the cloud  
 590 layer number from CALIPSO measurements; and (d) the expanded view of (b) for some cases  
 591 under single layer cloud situations.

592

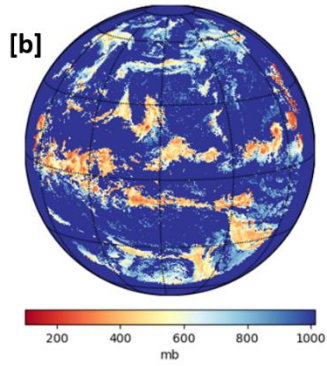
### 593 **3.3 Retrieval of global observation**

594 We applied our retrieval algorithm on the global DISCOVER EPIC measurement data at  
595 oxygen A and B bands. During the retrieval, only pixels with total cloud covering (i.e., cloud  
596 mask index of 4), surface albedo  $< 0.25$ , and [cloud optical depth COD](#)  $\geq 3$  are considered. To  
597 make the pictures easy to visualize and analyze, we set all invalid values are plot as white (or  
598 blank) pixels to 1013; same as the background sea level pressure.

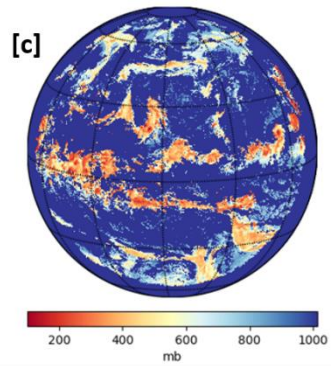
599 Figure [6a-8a](#) shows the synthesized RGB picture of EPIC measurements at GMT time  
600 00:17:51 on July 25, 2016. At this point in time the sun light covers most of the Pacific Ocean. In  
601 this figure, the white pixels represent cloud cover. Figure [6d-8b](#) shows the global [cloud optical](#)  
602 [depth COD](#) (NASA ASDC L2 data), in which the white areas and colorful areas indicate the clear  
603 sky areas and cloudy areas, respectively. On the whole, the highlights-cloudy areas are consistent  
604 with the RGB image. The highlight (red) areas indicate that the cloud systems there contain  
605 optically heavy clouds. Figure 8c shows the A-band effective CTP (NASA ASDC L2 data),  
606 where the white areas indicate clear sky or no valid values, warm (brown) and cold (blue) color  
607 areas indicate high-level and low-level clouds, respectively. According to the A-band effective  
608 CTP, the high-level clouds are dominant in the equatorial area, and the low-level clouds play a  
609 major role in the cloud systems in the Northern Pacific area. Figure [6b-8d](#) and [6e-8e](#) show the  
610 baseline and retrieved CTP at A-band, respectively, which also highlights-cloudy areas (white to  
611 brown) are consistent with the RGB image the A-band effective CTP image on the whole. Due to  
612 the filtering setting in the CTP retrieval algorithm, there are more white pixels (invalid values) in  
613 these two figures. The difference of A-band retrieved CTP and A-band effective CTP is shown in  
614 Figure 8d. The A-band retrieved CTP is overall smaller than A-band effective CTP, which  
615 difference is within 100 mb. The highlighted (brown or red) areas are located in the high level  
616 clouds areas or large COD areas. This indicates that the complexity of cloud system has  
617 significant impact on the CTP retrieval. Figure [6e-8g](#) and [6f8h](#) show the baseline and retrieved  
618 CTP in B-band respectively, which are similar to, but greater than the A-band. As shown in  
619 Figure 8i, the retrieved CTP at EPIC B-band is overall significantly larger than the retrieved CTP  
620 at EPIC A-band, which mean difference is up to 200 mb. Because we use the cloud optical depth  
621 to estimate the cloud pressure thickness in our retrieval, part of the retrieval error is from the  
622 cloud optical depth and the equation for cloud pressure thickness estimation.



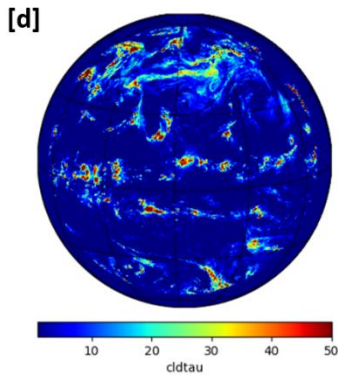
A-band Cloud TOP Pressure (baseline)



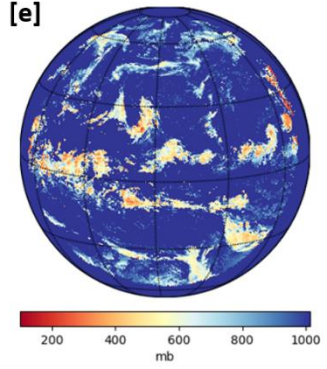
A-band Retrieved Cloud TOP Pressure



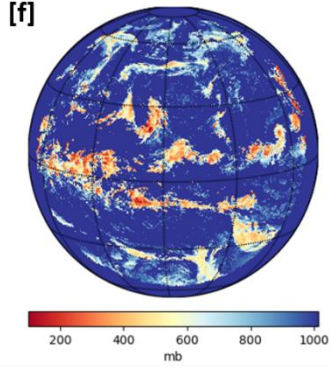
EPIC cloud tau



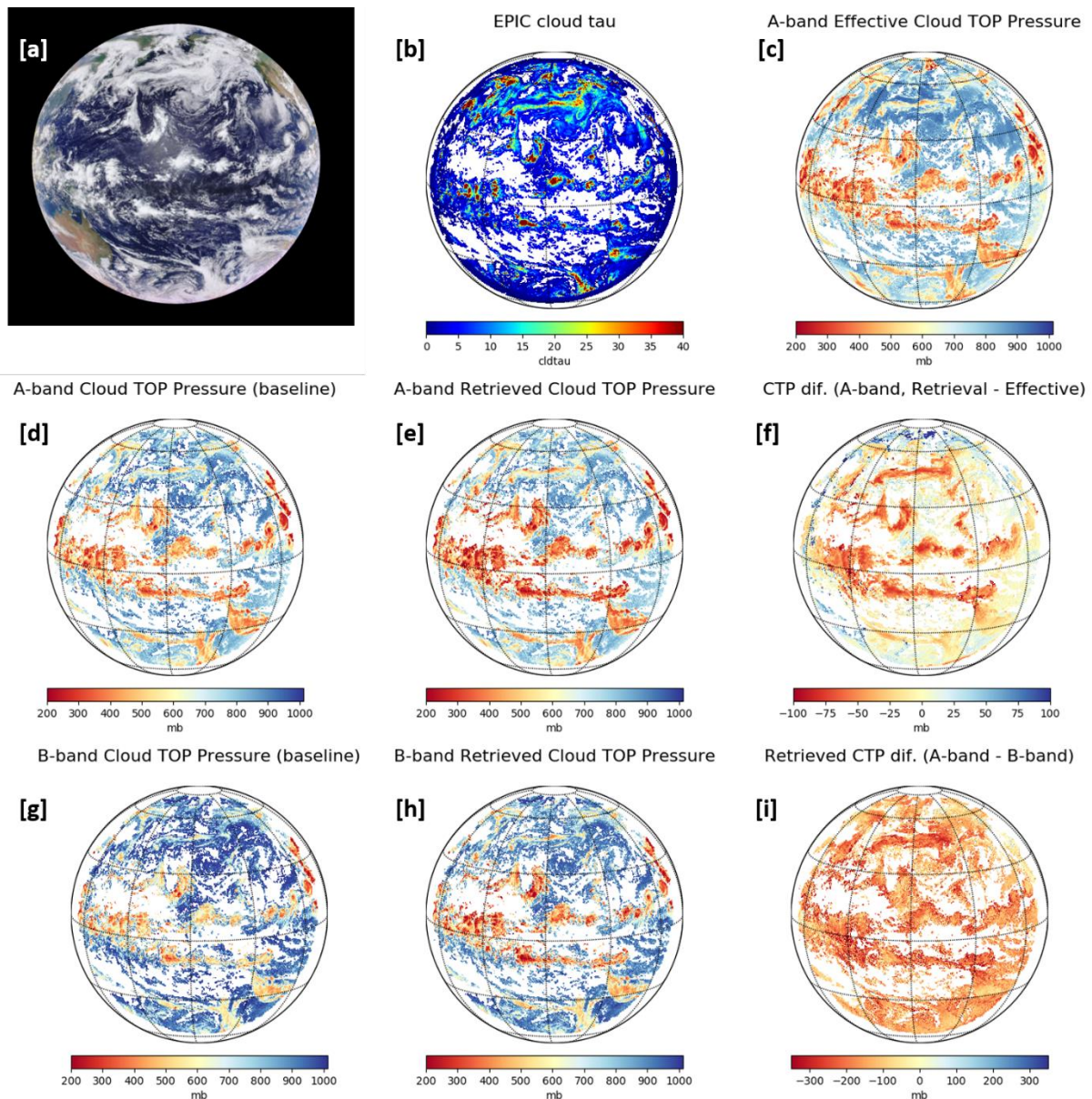
B-band Cloud TOP Pressure (baseline)



B-band Retrieved Cloud TOP Pressure



623



624

625 **Figure 68.** (a) RGB image from DSCOVER EPIC measurement at GMT time 00:17:51 on July  
 626 25, 2016; (b) and (c) COD (liquid assumption) and A-band effective CTP from NASA ASDC  
 627 EPIC L2 products; (d) and (e) Baseline and retrieved CTP derived from EPIC A-band  
 628 measurement. (d) Cloud optical depth (liquid assumption) from EPIC L2 products; (f) the  
 629 difference of A-band retrieved CTP and A-band effective CTP; (eg) and (fh) Baseline and  
 630 retrieved CTP derived from EPIC B-band measurement; and (i) the difference of retrieved CTP  
 631 between EPIC A-band and B-band.

632 As previously stated in the subsection 3.2: under single-layer cloud situations, the CTPs  
 633 derived from EPIC A-band measurements have good agreement with the CTP from CALIPSO  
 634 measurements; under multiple-layer cloud situations, the CTPs derived from EPIC  
 635 measurements may be larger than the CTPs of high level thin-clouds due to the effect of photon  
 636 penetration. Therefore, in the global range, for the large scale low-level stratus clouds, the  
 637 retrieved CTPs from EPIC A-band measurements should agree well with the actual value of

638 CTPs, but for the complex cloud system with multiple-layer clouds, the CTPs derived from EPIC  
639 A-band measurements may be larger than that of high level thin-clouds.

640

#### 641 2.4. Conclusion

642 The in-cloud photon penetration has significant impacts on the CTP retrieval when using  
643 DSCOVER EPIC oxygen A- and B- band measurements. To address this issue, we proposed two  
644 methods, (1) the LUT based method and (2) the analytic transfer inverse model method for CTP  
645 retrieval with consideration of in-cloud photon penetration. In the analytic transfer inverse model  
646 method, we build an analytic equation that represents the reflection at TOA from above cloud,  
647 in-cloud, and below-cloud, respectively. The coefficients of this analytic equation can be  
648 derived from a series of EPIC simulations under different atmospheric conditions using a non-  
649 linear regression algorithm. With EPIC observation data, the related solar zenith and sensor view  
650 angle, surface albedo data, cloud optical depth COD, and estimated cloud pressure thickness, we  
651 can retrieve the CTP by solving the analytic equation.

652 We developed a package for the DSCOVER EPIC measurement simulation. The high  
653 resolution radiation spectrum must be simulated first and then integrated with the EPIC filter  
654 function in order to accurately simulate EPIC measurements. Because this process is highly time-  
655 consuming, a polynomial fitting function is used when calculating the oxygen absorption  
656 coefficients under different atmospheric conditions. At the same time, the double-k approach is  
657 applied to do the high-resolution spectrum simulation to further reduce time-costs, which can  
658 obtain high accuracy results with hundred-fold time reduction. The results of the EPIC  
659 simulation measurements are consistent with theoretical analysis.

660 Based on the EPIC simulation measurements, we derived a series of coefficients from  
661 various solar zenith angles for the analytic EPIC equations. Using these coefficients, we  
662 performed CTP retrieval for real EPIC observation data. We have two kinds of retrieval results:  
663 baseline CTP and retrieved CTP. The baseline CTP is similar to the effective CTP in Yuekui  
664 Yang et al., (20122019), which does not consider cloud penetration. The retrieved CTP is  
665 derived by solving the analytic equation, with consideration of the in-cloud and below-cloud  
666 interactions. Compared to the effective CTP provided by NASA ASDC L2 data, the baseline  
667 CTP value at A-band is slightly higher, but the baseline CTP value at B-band is substantially  
668 higher. The retrieved CTP for both oxygen A- and B- bands is smaller than the related baseline  
669 CTP. At the same time, compared to the oxygen A-band, both baseline CTP and retrieved CTP at  
670 oxygen B-band is obviously larger. The cloud layer top pressure from CALIPSO measurements  
671 is used to validate the CTP derived from EPIC measurement. Under single-layer cloud situations,  
672 the retrieved CTPs for oxygen A-band agree well with the CTPs from CALIPSO, which mean  
673 difference is within 5 mb in the case study. Under multiple-layer cloud situations, the CTPs  
674 derived from EPIC measurements may be larger than the CTPs of high level thin-clouds due to  
675 the effect of photon penetration.

676 Currently, this analytical transfer model method can only retrieve CTP, and it still need  
677 cloud pressure thickness as an input parameter. However, in the satellite observations, both CTP  
678 and cloud pressure thickness are unknown. The estimation or assumption of cloud pressure

679 [thickness will bring in extra error in CTP retrieval. In the near future, we ~~will do further~~](#)  
680 [studiesplan](#) to address this issue.

## 681 **Acknowledgements [and Data](#)**

682 This work was supported partially by NASA's Research Opportunities in Space and Earth  
683 Science (ROSES) program element for DSCOVER Earth Science Algorithms managed by Dr.  
684 Richard Eckman, by the National Science Foundation (NSF) under contract AGS-1608735; and  
685 by the National Oceanic and Atmospheric Administration (NOAA) Educational Partnership  
686 Program with Minority Serving Institutions cooperative agreement #NA11SEC4810003.-[Dataset](#)  
687 [of DSCOVER EPIC Level 1B can be found in https://eosweb.larc.nasa.gov/project/dscovr/](#)  
688 [dscovr\\_epic\\_11b\\_2; dataset of EPIC Level 2 can be found in https://eosweb.larc.nasa.gov/](#)  
689 [project/dscovr/dscovr\\_epic\\_12\\_cloud\\_01; dataset of surface albedo from GOME can be found in](#)  
690 [http://temis.nl/surface/gome2\\_ler/databases/; dataset of cloud layer data from CALIPSO can be](#)  
691 [found in https://eosweb.larc.nasa.gov/project/calipso/cal\\_lid\\_12\\_05kmclay\\_standard\\_v4\\_20.](#)

692

## 693 **Reference**

694 [Bodhaine, B.A., Wood, N.B., Dutton, E.G. and Slusser, J.R.: On Rayleigh optical depth](#)  
695 [calculations. Journal of Atmospheric and Oceanic Technology, 16\(11\), pp.1854-1861, 1999.](#)

696 [Carbajal Henken, C. K., Doppler, L., Lindstrot, R., Preusker, R., and Fischer, J.: Exploiting the](#)  
697 [sensitivity of two satellite cloud height retrievals to cloud vertical distribution, Atmos. Meas.](#)  
698 [Tech., 8, 3419–3431, https://doi.org/10.5194/amt-8-3419-2015, 2015.](#)

699 Chandrasekhar, S.: Radiative transfer. Dover, New York, 1960.

700 Chou, M.D. and Kouvaris, L.: Monochromatic calculations of atmospheric radiative transfer due  
701 to molecular line absorption. Journal of Geophysical Research: Atmospheres, 91(D3), pp.4047-  
702 4055, 1986.

703 Clough, S. A., Shephard, M. W., Mlawer, E. J., Delamere, J. S., Iacono, M. J., Cady-Pereira, K.,  
704 Boukabara, S., and Brown, P.D.: Atmospheric radiative transfer modeling: a summary of the  
705 AER codes, Short Communication, J. Quant. Spectrosc. Ra., 91,233–244, 2005.

706 Daniel, J.S., Solomon, S., Miller, H.L., Langford, A.O., Portmann, R.W. and Eubank, C.S.:  
707 Retrieving cloud information from passive measurements of solar radiation absorbed by  
708 molecular oxygen and O2-O2. Journal of Geophysical Research: Atmospheres, 108(D16), 2003.

709 [Dannenberg, Roger B.: Interpolation error in waveform table lookup, In Proceedings of the](#)  
710 [International Computer Music Conference. San Francisco: International Computer Music](#)  
711 [Association, 1998.](#)

712 Davis, A.B., Merlin, G., Cornet, C., Labonnote, L.C., Riédi, J., Ferlay, N., Dubuisson, P., Min,  
713 Q., Yang, Y. and Marshak, A.: Cloud information content in EPIC/DSCOVER's oxygen A-and B-  
714 band channels: An optimal estimation approach. Journal of Quantitative Spectroscopy and  
715 Radiative Transfer, 216, pp.6-16, 2018a.

716 Davis, A.B., Ferlay, N., Libois, Q., Marshak, A., Yang, Y. and Min, Q.: Cloud information  
717 content in EPIC/DSCOVR's oxygen A-and B-band channels: A physics-based approach. *Journal*  
718 *of Quantitative Spectroscopy and Radiative Transfer*, 220, pp.84-96, 2018b.

719 Davis, A.B. and Marshak, A.: Space-time characteristics of light transmitted through dense  
720 clouds: A Green's function analysis. *Journal of the atmospheric sciences*, 59(18), pp.2713-2727,  
721 2002.

722 Duan, M., Min, Q. and Li, J.: A fast radiative transfer model for simulating high-resolution  
723 absorption bands. *Journal of Geophysical Research: Atmospheres*, 110(D15), 2005.

724 Ferlay, N., Thieuleux, F., Cornet, C., Davis, A.B., Dubuisson, P., Ducos, F., Parol, F., Riédi, J.  
725 and Vanbauce, C.: Toward new inferences about cloud structures from multidirectional  
726 measurements in the oxygen A band: middle-of-cloud pressure and cloud geometrical thickness  
727 from POLDER-3/PARASOL. *Journal of Applied Meteorology and Climatology*, 49(12),  
728 pp.2492-2507, 2010.

729 Fischer, J. and Grassl, H.: Detection of cloud-top height from backscattered radiances within the  
730 oxygen A band. Part 1: Theoretical study. *Journal of Applied Meteorology*, 30(9), pp.1245-1259,  
731 1991.

732 [Gastellu-Etchegorry, J.P., Gascon, F. and Esteve, P.: An interpolation procedure for generalizing  
733 a look-up table inversion method. \*Remote Sensing of Environment\*, 87\(1\), pp.55-71, 2003.](#)

734 [Gelaro, R., McCarty, W., Suárez, M.J., Todling, R., Molod, A., Takacs, L., Randles, C.A.,  
735 Darmenov, A., Bosilovich, M.G., Reichle, R. and Wargan, K.: The modern-era retrospective  
736 analysis for research and applications, version 2 \(MERRA-2\). \*Journal of Climate\*, 30\(14\),  
737 pp.5419-5454, 2017.](#)

738 [Geogdzhayev, I. and Marshak, A.: Calibration of the DSCOVR EPIC visible and NIR channels  
739 using MODIS Terra and Aqua data and EPIC lunar observations. \*Atmos. Meas. Tech.\* 11, 359 -  
740 368, <https://doi.org/10.5194/amt-11-359-2018>, 2018](#)

741 Gordon, I.E., Rothman, L.S., Hill, C., Kochanov, R.V., Tan, Y., Bernath, P.F., Birk, M., Boudon,  
742 V., Campargue, A., Chance, K.V. and Drouin, B.J.: The HITRAN2016 molecular spectroscopic  
743 database. *Journal of Quantitative Spectroscopy and Radiative Transfer*, 203, pp.3-69, 2017.

744 Holdaway, D. and Yang, Y.: Study of the effect of temporal sampling frequency on DSCOVR  
745 observations using the GEOS-5 nature run results (Part II): Cloud Coverage. *Remote*  
746 *Sensing*, 8(5), p.431, 2016.

747 Ishimaru, A.: Wave propagation and scattering in random media. Wiley-IEEE-Press, New York,  
748 1999.

749 Irvine, W. M: The formation of absorption bands and the distribution of photon optical paths in a  
750 scattering atmosphere. *Bull. Astron. Inst. Neth.*, 17, 266-279, 1964.

751 Ivanov, V. V., and S. D. Gutshabash, 1974: Propagation of brightness wave in an optically thick  
752 atmosphere. *Phys. Atmos. Okeana*, **10**, 851-863.

753 Koелеmeijer, R.B.A., Stammes, P., Hovenier, J.W. and Haan, J.D.: A fast method for retrieval of  
754 cloud parameters using oxygen A band measurements from the Global Ozone Monitoring  
755 Experiment. *Journal of Geophysical Research: Atmospheres*, 106(D4), pp.3475-3490, 2001.

756 [Kokhanovsky, A. A. and Rozanov, V. V.: The physical parameterization of the top of-](#)  
757 [atmosphere reflection function for a cloudy atmosphere–underlying surface system: the oxygen](#)  
758 [A-band case study. \*Journal of Quantitative Spectroscopy and Radiative Transfer\*, 85, 35–55,](#)  
759 [doi:10.1016/S0022-4073\(03\)00193-6, 2004.](#)

760 Kokhanovsky, A. A., Rozanov, V. V., Zege, E. P., Bovesmann, H., and Burrows, J. P.: A semi  
761 analytical cloud retrieval algorithm using backscattered radiation in 0.4–2.4  $\mu\text{m}$  spectral region,  
762 *J.Geophys. Res.*, 108, 4008, doi:10.1029/2001JD001543, 2003.

763 Kuze, A. and Chance, K.V.: Analysis of cloud top height and cloud coverage from satellites  
764 using the O2 A and B bands. *Journal of Geophysical Research: Atmospheres*, 99(D7), pp.14481-  
765 14491, 1994.

766 [Lelli L, Kokhanovsky, A.A., Rozanov, V.V., Vountas M., and Burrows, J.P.: Linear trends in](#)  
767 [cloud top height from passive observations in the oxygen A-band, \*Atmospheric Chemistry and\*](#)  
768 [\*Physics\*, 14, 5679-5692, doi:10.5194/acp-14-5679-2014, 2014.](#)

769 [Lelli L, Kokhanovsky, A.A., Rozanov, V.V., Vountas M., Sayer, A.M., and Burrows, J.P.: Seven](#)  
770 [years of global retrieval of cloud properties using space-borne data of GOME, \*Atmospheric\*](#)  
771 [\*Measurement Techniques\*, 5, 1551-1570, doi:10.5194/amt-5-1551-2012, 2012.](#)

772 [Loyola, D. G., Gimeno García, S., Lutz, R., Argyrouli, A., Romahn, F., Spurr, R. J. D.,](#)  
773 [Pedernana, M., Doicu, A., Molina García, V., and Schüssler, O.: The operational cloud retrieval](#)  
774 [algorithms from TROPOMI on board Sentinel-5 Precursor, \*Atmos. Meas. Tech.\*, 11, 409–427,](#)  
775 [https://doi.org/10.5194/amt-11-409-2018, 2018.](#)

776 Marshak, A., and Davis, A. (Eds.): 3D radiative transfer in cloudy atmospheres. Springer  
777 Science & Business Media, 2005.

778 Marshak, A., Herman, J., Adam, S., Carn, S., Cede, A., Geogdzhayev, I., Huang, D., Huang,  
779 L.K., Knyazikhin, Y., Kowalewski, M. and Krotkov, N.: Earth observations from DSCOVR  
780 EPIC instrument. *Bulletin of the American Meteorological Society*, 99(9), pp.1829-1850, 2018.

781 Meyer, K., Yang, Y. and Platnick, S.: Uncertainties in cloud phase and optical thickness  
782 retrievals from the Earth Polychromatic Imaging Camera (EPIC). *Atmospheric measurement*  
783 *techniques*, 9(4), p.1785, 2016.

784 [Min, Q. and Harrison, L.C.: Retrieval of atmospheric optical depth profiles from downward-](#)  
785 [looking high-resolution O2 A-band measurements: Optically thin conditions. \*Journal of the\*](#)  
786 [\*atmospheric sciences\*, 61\(20\), pp.2469-2477, 2004.](#) [Min, Q.L., Harrison, L.C., Kiedron, P.,](#)  
787 [Berndt, J. and Joseph, E.: A high-resolution oxygen A-band and water vapor band](#)  
788 [spectrometer. \*Journal of Geophysical Research: Atmospheres\*, 109\(D2\), 2004.](#)

789 Min, Q., Yin, B., Li, S., Berndt, J., Harrison, L., Joseph, E., Duan, M. and Kiedron, P.: A high-  
790 resolution oxygen A-band spectrometer (HABS) and its radiation closure. *Atmospheric*  
791 *Measurement Techniques*, 7(6), pp.1711-1722, 2014.

792 O'brien, D.M. and Mitchell, R.M.: Error estimates for retrieval of cloud-top pressure using  
793 absorption in the A band of oxygen. *Journal of Applied Meteorology*, 31(10), pp.1179-1192,  
794 1992.

795 Pandey, P., Ridder, K.D., Gillotay, D. and Van Lipzig, N.P.M.: Estimating cloud optical  
796 thickness and associated surface UV irradiance from SEVIRI by implementing a semi-analytical  
797 cloud retrieval algorithm. *Atmospheric Chemistry and Physics*, 12(17), pp.7961-7975, 2012.

798 [Preusker, R. and Lindstrot, R.: Remote Sensing of Cloud-Top Pressure Using Moderately](#)  
799 [Resolved Measurements within the Oxygen A Band-A Sensitivity Study, \*J. Appl. Meteorol.\*](#)  
800 [\*Clim.\*, 48, 1562–1574, 2009.](#)

801 [Richardson, M. and Stephens, G.L.: Information content of OCO-2 oxygen A-band channels for](#)  
802 [retrieving marine liquid cloud properties. \*Atmospheric Measurement Techniques\*, 11\(3\),](#)  
803 [pp.1515-1528, 2018.](#)

804 [Rozanov, V. V. and Kokhanovsky, A. A.: Semianalytical cloud retrieval algorithm as applied to](#)  
805 [the cloud top altitude and the cloud geometrical thickness determination from top-of-atmosphere](#)  
806 [reflectance measurements in the oxygen A band, \*Journal of Geophysical Research:\*](#)  
807 [\*Atmospheres\*, 109, 4070, doi:10.1029/2003JD004104, 2004.](#)

808 Schuessler, O., Rodriguez, D.G.L., Doicu, A. and Spurr, R.: Information Content in the Oxygen  
809 A-Band for the Retrieval of Macrophysical Cloud Parameters. *IEEE Transactions on Geoscience*  
810 *and Remote Sensing*, 52(6), pp.3246-3255, 2013.

811 [Seager, S., Turner, E.L., Schafer, J. and Ford, E.B.: Vegetation's red edge: a possible](#)  
812 [spectroscopic biosignature of extraterrestrial plants. \*Astrobiology\*, 5\(3\), pp.372-390, 2005.](#)

813 Stamnes, K., Tsay, S.C., Wiscombe, W. and Jayaweera, K.: Numerically stable algorithm for  
814 discrete-ordinate-method radiative transfer in multiple scattering and emitting layered  
815 media. *Applied optics*, 27(12), pp.2502-2509, 1988.

816 Thomas, G. E., and Stamnes, K.: Radiative transfer in the atmosphere and ocean. Cambridge  
817 University Press, Cambridge, 2002.

818 Tilstra, L.G., Wang, P. and Stamnes, P.: Surface reflectivity climatologies from UV to NIR  
819 determined from Earth observations by GOME-2 and SCIAMACHY. *Journal of Geophysical*  
820 *Research: Atmospheres*, 122(7), pp.4084-4111, 2017.

821 Van de Hulst, H. C.: Multiple Light Scattering: Tables, Formulas, and Applications. Academic  
822 Press, 299 pp, 1980.

823 Van de Hulst HC.: Multiple light scattering: tables, formulas, and applications. Elsevier; 2012.

824 [Yamamoto, G. and Wark, D. Q.: Discussion of letter by A. Hanel: determination of cloud](#)  
825 [altitude from a satellite, \*Journal of Geophysical Research: Atmospheres\*, 66, 3596, 1961.](#)

826 [Vaughan, M.A., Young, S.A., Winker, D.M., Powell, K.A., Omar, A.H., Liu, Z., Hu, Y. and](#)  
827 [Hostetler, C.A.: November. Fully automated analysis of space-based lidar data: An overview of](#)  
828 [the CALIPSO retrieval algorithms and data products. In \*Laser radar techniques for atmospheric\*](#)  
829 [\*sensing\* \(Vol. 5575, pp. 16-30\). International Society for Optics and Photonics, 2004.](#)

830 Yang, Y., Marshak, A., Mao, J., Lyapustin, A. and Herman, J.: A method of retrieving cloud top  
831 height and cloud geometrical thickness with oxygen A and B bands for the Deep Space Climate  
832 Observatory (DSCOVR) mission: Radiative transfer simulations. *Journal of Quantitative*  
833 *Spectroscopy and Radiative Transfer*, 122, pp.141-149, 2013.

834 Yang, Y., Meyer, K., Wind, G., Zhou, Y., Marshak, A., Platnick, S., Min, Q., Davis, A.B.,  
835 Joiner, J., Vasilkov, A. and Duda, D.: Cloud products from the Earth Polychromatic Imaging  
836 Camera (EPIC): algorithms and initial evaluation. *Atmospheric Measurement Techniques*, 12(3),  
837 2019.

838

839